Heliyon 10 (2024) e29554

Contents lists available at ScienceDirect

Heliyon

journal homepage: www.cell.com/heliyon

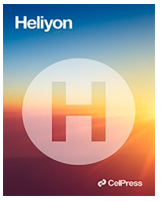

Research article

Appraisal of reservoir quality for hydrocarbon-bearing deep-water Miocene sandstones incised valley, south-east Asian offshore Indus: An application of seismic attributes and instantaneous spectral porosity quantitative reservoir simulations

Muhammad Tayyab Naseer [a,b,c,*], Abha Singh [e], Raja Hammad Khalid [b], Shazia Naseem [b], Ilyas Khan [d], George Kontakiotis [f]

[a] Exploration Department, MOL Pakistan Oil and Gas Co. B.V., Pakistan
[b] Department of Earth Sciences, Quaid-I-Azam University, Islamabad, Pakistan
[c] Solid Earth Geophysics Division (SEGD), Center for Earth Quakes (CES) National Center for Physics (NCP), Quaid-I-Azam University Campus, Islamabad, Pakistan
[d] Department of Mathematics, College of Science Al-Zulfi, Majmaah University, Al-Majmaah, 1952, Saudi Arabia
[e] Department of Basic Sciences, College of Sciences and Theoretical Studies, Dammam-branch, Saudi Electronic University, Riyadh, Saudi Arabia
[f] Department of Historical Geology-Paleontology, Faculty of Geology and Geoenvironment, School of Earth Sciences, National and Kapodistrian University of Athens, Panepistimiopolis, Zografou, 15784, Athens, Greece

ARTICLE INFO

Keywords:
Deep-water depositional sequences
Conventional seismic data
45-Hz-based processing
Coarse-grained sandstone deposits

ABSTRACT

Incised marine valleys (IVS) are hot topics in exploring the stratigraphic oil and gas-bearing plays. Multiple channelized sandstone lenses at varying depths [m], thicknesses [m], and porosities [%] constrain seismic impedance. The presence of hydrocarbon-bearing resources affects the seismic impedance (density (g/cc) and velocity (m/s)). Therefore, a quantitative prediction has been carried out for determining the thickness [m], porosity [%], and depths [m] of laterally distributed channelized sandstone lenses (SLS) for IVS, Indus offshore Basin (IOB), Pakistan, using 2-D instantaneous spectral porosity quantitative modelling (2DSSM), continuous wavelet transforms-based (CWT) 2-D instantaneous spectral density modelling (2DSSDM), and spectral decomposition tools. The 2DSSM remained limited in predicting the number of channelized sandstone lenses and their quantitative stratigraphic attributes. The 45-Hz-based processing of conventional 2DSSM has resolved the two channelized sandstone lenses of the stratigraphic trap. The deepest channelized sandstone lens has attained 1–6 m thickness with a lateral extent of 3 km, within the porosity range of 18–33 %. The highest confidence level for predicted petrophysical attributes such as 13 m-thick pay zones, −0.08, −0.067, and −0.07 acoustic impedances [g/c.c.*m/s], and 28 % porosities with $R^2 > 0.85$ have validated interpretations. The response of 45-Hz CWT waveform-based inverted density and thickness simulations has predicted the highest thicknesses and lowest densities of reservoir sandstones within the meandering channel belt of the deepwater depositional system. The predicted densities and thicknesses for the coarse-grained sandstone lenses of point bars were 1.8–1.9 g/cc and 15 m, respectively. In the same way, the quantitative estimates of predicted density and simulated thickness have shown a strong coefficient correlation ($R^2 > 0.80$), which confirms the presence of gas-bearing prospects within the

* Corresponding author. Mol Pakistan Oil and Gas Co. B.V. Pakistan.
E-mail addresses: mtayyab.naseer1@gmail.com (M.T. Naseer), i.said@mu.edu.sa (I. Khan).

https://doi.org/10.1016/j.heliyon.2024.e29554
Received 24 October 2023; Received in revised form 9 April 2024; Accepted 10 April 2024
Available online 16 April 2024

IVS. The facies-controlled migration is thought to be the movement of the reservoir facies of the point bars and channelled sandstone-filled lenses to the side.

1. Introduction

Incised marine valleys (IVS) are important indicators of base-level changes on continental shelves during the low sea level of the Quaternary [1–3]. It produces a depositional space mainly from fluvial erosion which is filled by fluvial-, tide-derived material, and influenced by wave processes [4]. The IVS may be completely or partially filled, containing deposits of the following transgressions and high-stands [5], supplementary to those deposited before the flooding [6–10]. The practical implications for achieving oil and gas exploration are to identify the geometry of the IVS, including their architecture and their lithological types for gas exploration [11]. Seismic attributes and spectrum decay remain modern seismic analysis tools that help in mapping channelized reservoirs [12,13]. Reservoir characterization helps to identify the lithology and fluids inside the diversified depositional systems [14–29]. There are various researchers in the field of explorations, who have applied various tools for the diversity of sub-surface stratigraphy, geology, structural analysis and reservoir engineering tools. These techniques have been confined to confining pressures of porous rock, suitable marine–continental transitional shales, velocity and spectral acceleration tools for the identification of continental shale, wavelet-based analysis for assessing the precipitation and river discharge compaction and cracking of porous cracked rocks [28, 30–36]. The reflection from thin-bedded strata tends to show a distinctive response within the time-frequency analysis, which can be used to infer the vertical resolvable strata. This technique has validated its successful oil and gas discoveries by describing and quantitatively visualizing the stratigraphy of the hydrocarbon-bearing sub-surface systems [12,37–42] up to standards that were not possible to be reached using conventional analysis tools. Additionally, it remained a robust tool for geo-hazardous analysis due to its enhanced sensitivity towards waveform, reflection, tuning-based effects, and fluctuations in the reservoirs as caused by the attenuation phenomenon [43]. The process of decomposition splits the conventional amplitudes of sub-surface reservoirs into their frequency-dependent amplitude volumes. Therefore, analyzing the distinct comparison of frequency constituents helps in inferring the geological aspects of the sub-surface petroleum plays. Although the maps generated using this tool has been a non-unique procedure, there are numerous approaches aimed at implementing this analysis of the non-static signal. In the petroleum industry, the dominant tools include the Fourier transform (FFT), continuous wavelet transform (CWT), S-transform (ST), and matching pursuit decomposition (MPD). Each one of these methods has its outcomes and drawbacks [44,45]. In all these approaches, the CWT remains the exceptional device for achieving enhanced frequency determination on inferior frequencies and time determination at higher frequency panels. Consequently, CWT has applied cutting-edge training toward predicting the quantifiable characteristics of IVS in the Indus Offshore Basin (IOB) in Pakistan.

The Indus Offshore Basin (IOB), was previously analyzed for structural and stratigraphic exploration for hydrocarbon-bearing shows [46,47]. Recent studies relying on sequence stratigraphic attributes have revealed possible locations for the exploration of the hydrocarbon trapping areas within the IOB. These studies have initiated a new era of exploration within the IOB of Pakistan, focusing mostly on the most promising zones (particularly from slope to deepwater basin floor fans between ~10 km distance away from the sedimentary proximal position) for economic development within the IOB [48–51]. Moreover, additional studies were conducted for stratigraphic traps of low-stand prograding wedge plays. The porosity modelling was performed to predict the porous and thickest reservoirs inside the IOB [52,53]. However, reservoir characterization was not done comprehensively during the last three decades. In the most recent workflow, the basin floor fans were characterized using static reservoir properties, such as constant density and velocity-based wedge modelling. The key issue of that attempt was the exact prediction of densities and velocities, which ultimately impacts the porous segments of the reservoir segments [54]. In their attempt to resolve the thin-bedded stratigraphic traps, these researchers used the DAS-based post-processing tool. This tool was quite enough to image the geomorphology, but still, the exact porosities and densities were not simulated, which could have surely predicted the exact extent and the reservoir attributes based on the presented inverted reservoir simulation workflows. During the development of IVS, the channelized sandstone lenses (USL) are deposited during relative falling sea level and succeeding growth along an extensional or compressional regime. A series of channel-levee systems (SLS) has made a vital impact on the development of IVS. However, these wedge plays were present at deeper reservoir zones compared to the current study, dealing with a depth range of 3600–3625 m. The dominant reservoir within this zone is the complex channel system, which fills the IVS with coarse-grained sandstone deposits. During the development of IVS, the series of SLS are deposited throughout the falling sea with insignificant growth. Within borehole environments, pressure and stress are vitally controlled by velocity and porosity. These parameters are two vital tools that can be used to predict lithology, porosity, and accommodation space [52,53]. Hence, the prediction of fewer compact zones with high porosity and low density can lead to the accumulation of hydrocarbon-bearing reserves. As the velocity and density increase, the compaction increases, which reduces the porosity of the rock matrix. On the contrary, the reduction in velocity and density increases the porosity of the rock matrix, which leads to the development of the pore space to accumulate the porous reservoir facies. Additionally, the SLS inside the IVS are thin-bedded stratigraphic traps. The IVS presents highly discontinuous reflections using full-spectrum data. If compressional zones are delineated, there are more chances for the loss of porous sandstone facies. Therefore, they require a significant magnitude of frequency, which can be used to predict the exact position, thickness, lateral distribution, and porosity for the extensional and compressional regimes. The reflection-based impedance is the product of density (g/c.c) and velocity (m/s), which in conjunction with the porosity, could reveal the quantitative-based stratigraphic attributes of the gas-bearing plays. These stratigraphic attributes include depositional trends, thickness, lateral extent, fracture density, porosity, extensional and compressional regimes, as well as the different types of

depositional facies that are accumulated under these geological conditions [11]. Consequently, considering the above geological parameters, this study makes an original contribution through the usage of the 2-D instantaneous spectral porosity quantitative modelling (2DSSM), CWT-based 2-D instantaneous spectral density modelling (2DSSDM), and spectral decomposition tool to emphasize the reservoir quality for stratigraphic traps in extensional regimes.

2. Geological setting

The Indus offshore region has been subject to little exploration within the stratigraphic consortium. Several boreholes have been successfully sunk in the offshore region of the Indus River. Currently, three of these boreholes are still operational in deep-water areas. The efforts made in this endeavours proved to be unproductive since all these wells encountered high-pressure conditions within the Miocene stratigraphic area. The assessment of hydrocarbon plays and non-commercial gas quantities has been conducted via the Pakistan Petroleum Information Services web platform [11]. The north-western portions adjacent to the Murray Ridge (MR) serve as the primary boundary for the Indus Offshore Basin (IOB) in Pakistan (Fig. 1a).

The rise of the tectonic plate in the Gulf of Aden during the Late Oligocene/Early Miocene period [46,47] led to the development of a transform fault. The resulting faulted blocks are comprised of a vertical and strike-slip faulted assemblage, which is further characterized by parallel blocks that move in a west-east direction along transform faults. A multitude of channel-levee complexes are observed inside petroleum-bearing zones. The Miocene sedimentary succession exhibits different intervals that reflect the potentiality of conducting oil and gas exploration in the channel-levee systems (CLS) [11] (see Fig. 1b). The field of tectonics has had a significant influence on the investigation of such hydrocarbon-bearing systems. The IOB has a significant presence of pure stratigraphic traps in the form of wedges, which possess a high reservoir quality characterized by a porosity of 25 % [52,53]. The primary categories of reservoir trapping consist of stratigraphic traps located along the MR, as well as folded rock units that are connected to the lateral *trans*-forms and strike-slip faults [47].

The passive border of the Basin is characterized by the presence of channel-levee systems (SLS) that include stratigraphically based oil and gas-bearing traps throughout the Miocene and Oligocene-to-Recent geological periods. These traps have been formed by the accumulation of siliciclastic sediments, which originate from and are produced by the Indus deepwater turbidite system [47]. Traps consist of rollover anticlines that converge from extensional to local settings on the margin of the shelf, forming draped assemblages. The stratigraphic traps have a lateral distribution along the Murray Ridge and present a folded architecture, which is correlated with the presence of strike-slip faults along the same ridge [47]. The examination of the low-stand system tract (LST) reveals the characteristics of deep-water architecture, which includes the basin floor fans (BFF), slope fans (SF), and low-stand prograding wedge (LPW), respectively.

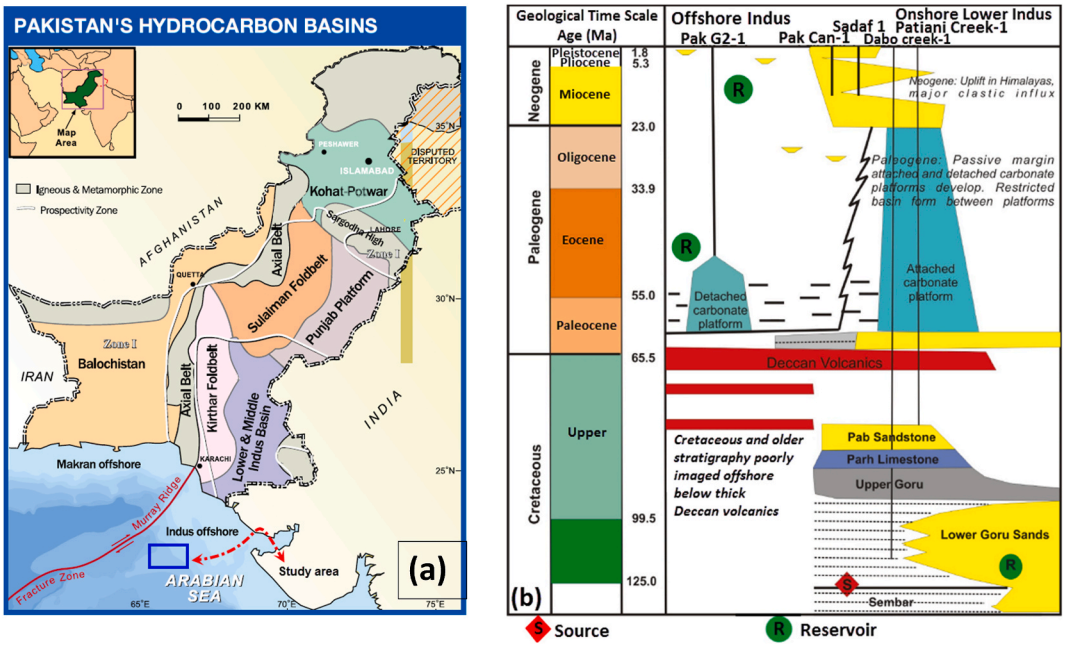

Fig. 1. **(a)** Topographical position of the OIB, denoting the examination area (blue-coloured block) as shown by the red-coloured dashed-arrow, and its site relative to the Indian Ocean remnants exposed cutting-edge the lowermost accurate place, Pakistan; **(b)** Comprehensive stratigraphic divisions of the research area, displaying the dissemination of pool interims.

3. Material and methods

This investigation utilized 2D high-resolution seismic profiles, comprising two dip lines and one strike line, as illustrated in Fig. 2a. The reservoir zone consists of Miocene sedimentary stages that are characterized by intricate structures due to vertical stacking patterns, which usually lose their connectivity and provide constraints for channelized sandstone deposits to quantify them for petroleum exploration [47]. The CWT tool was applied to a NE-SW oriented seismic profile, spanning a length of 78 km (Fig. 2b), using a frequency range of 26–60 Hz. The seismic survey encompassed a total area of 8000 square kilometres. The SEG format was employed to preserve the dataset within a geophysical software tool. If the data is processed within the defined bandwidth within the exploration zones, then all the noise events are removed and the highest signals are enhanced. In this way, the interpretation of thin-bedded petroleum-bearing reservoirs becomes easier as they are detected at their right sub-surface locations and depths. Otherwise, the shales of non-reservoir zones will result in the illumination of bright amplitude, which would be not due to the presence of hydrocarbons, but to the water of other non-reservoir fluids. Therefore, once the bandwidth is defined and the CWT is processed, as

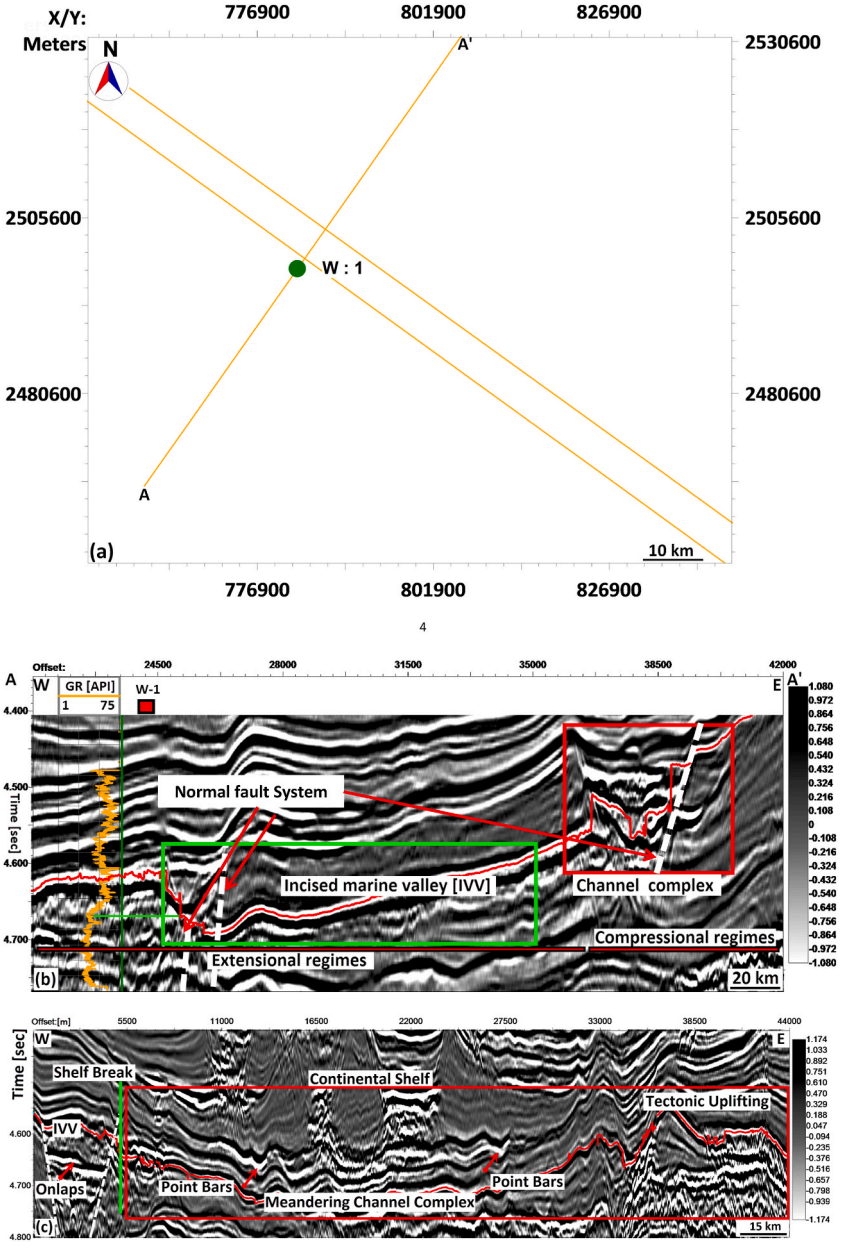

Fig. 2. (**a**) The 2-D seismic survey was acquired to image and characterize the incised marine valleys (IVS); (**b**) Seismic amplitude sections for IVS, showing the interpreted reservoir (IVS), geomorphology of the complex channel system, and normal fault system.

performed in the reservoir simulations, the results will be suitable for extracting information for thickness, lithology, angle of trap, and other quantitative-based attributes. Therefore, the inverted reservoir simulations are performed to predict the unknown parameters such as the paleo-thickness, paleo-densities, and paleo-velocities, (Figs. 4, 5 and 7). The vertical seismic resolution threshold was calculated for the time interval ranging from 4.4 to 4.7 s. A velocity of 1620 m/s was employed, required for time-depth conversion and tuning analysis. The vertical seismic threshold required to effectively distinguish the thin-bedded combination traps was determined to be 9 m. Therefore, the sandstone formation measuring 25 m in depth (from 3600 to 3625 m) was utilized. The gamma-ray (GR) API, the compressional wave travel time (DT) in microseconds per foot, and the bulk density (Rhob) in grams per cubic centimetre were utilized in the construction of the geomechanical models. The dataset was restricted to publicly available information. The seismic data exhibited a satisfactory level of density; nevertheless, the scarcity of well controls imposed constraints on the interpretation of the seismic data. Consequently, the inverted reservoir simulations were exclusively conducted with the data of only one single well. Tables 1–4 show the complete range of QC parameters of the seismic datasets used for this work, and the quantitative-based estimations of the reserovir attributes for the deep-water depositional system.

3.1. Seismic attributes

The advancement of seismic imaging methods has significantly contributed to the exploration of various structural and stratigraphic reservoirs [13,52,55–57]. The primary objective of stratigraphic exploration is the identification and refinement of the optimal amalgamation of attributes that can offer comprehensive insights into the distinctive features of reservoirs containing oil and gas. The current investigation employed seismic amplitude, instantaneous frequency, relative acoustic impedance, and spectral decomposition features for reservoir characterization.

3.2. Instantaneous frequency

The temporal component of seismic phases with one another, i.e., the degree of alteration of the timing, is the simultaneous frequencies.

$$F(t) = d(\Phi(t))/dt \quad \text{(Eq. 1)}$$

According to Taner [58], the simultaneous frequencies are characterized as the temporal variation of concurrent phases. The object in question is a tangible asset that indicates the presence of petroleum and gas reservoirs, as well as fracture networks. This is achieved by analyzing the lithography, depositional settings, and acoustic morphologies of thin-bedded hydrocarbons that exhibit truncation frequencies [58–61].

3.3. The relative acoustic impedance (RAI) inversion

The determination of RAI involved the utilization of a consistent blend of initial geological signals and subsequent low-cut filtering demands. The objective of carryout may be easily identified if the contents of the RAI are analyzed within the designated seismic frequency range [59]. The integration of zero-phased tracing leads to a constrained estimation of typical artificial intelligence recordings inside a certain group.

3.3.1. Computation of RAI volumes

The calculations are an essential summation that includes lower band sorting, without a comprehensive reversal. It symbolizes the material characteristic comparison, and consequently, it's a physical characteristic that is being effectively employed in multiple measurement methods (Kingdom 8.6 2011). The RAI is a simple reversion [62].

$$f(t) = 1/2 \triangle \rho v/\rho v \quad \text{(Eq. 2)}$$

$$f(t) = 1/2 \triangle \ln\text{-}(\rho v). \quad \text{(Eq. 3)}$$

Table 1
Comprehensive seismal acquirement constraints of OIB, SW Pakistan (Naseer et al., 2023).

	TOTAL EXPLORATION PAKISTAN INDUS OFFSHORE BLOCKS G & H
1.	RECORDED BY FUGRO GEOTEAM NOVEMBER - DECEMBER 2000
2.	REEL: 10SFMIG2 DATASET: FINAL FILTERED AND SCALED MIGRATION
3.	VESSEL: R/V GEO BALTIC; SHOOTING DIRECTION 127 DEGREES
4.	DATA TRACES/RECORD: 480; AUXILIARY TRACES/RECORD: 0 CDP FOLD: 80
5.	SAMPLE INT: 2 MS; SAMPLES/TRACE: 2561
6.	RECORDING FORMAT: SEG-D 8015; FORMAT THIS REEL: SEG-Y
7.	RECORDING FILTER: 4 HZ (18 DB/OCT) - 206 HZ (266 DB/OCT)
8.	SOURCE: AIRGUN ARRAY; SP INTERVAL: 37.5 M
9.	NEAR OFFSET: 143 M; CABLE LENGTH: 6000 M; GROUP INT: 12.5 M
10.	TRACES SORTED BY CDP

Table 2
Comprehensive seismal processing constraints of OIB, SW Pakistan (Naseer et al., 2023).

S.No	Physical Parameterization
1.	VERITAS DGC LTD, DECEMBER 2000 - JUNE 2001
2.	REFORMAT FROM SEG-D AND EDIT
3.	DEPHASE AND ANTI-ALIAS FILTER, RESAMPLE TO 4 MS
4.	6HZ 18DB/OCT LOW CUT FILTER 2D NAVIGATION ASSIGNMENT
5.	BACK OUT DEPHASE FILTER REAPPLY ZERO PHASING FILTER WITH RECEIVER GHOST
6.	SPHERICAL DIVERGENCE CORRECTION - T IN WATER LAYER V SQUARED T IN DATA
7.	CREATE 240-FOLD SUPERGATHER NMO CORRECT WITH MULTIPLE VELOCITY FUNCTION
8.	500MS AGC RADON DEMULTIPLE - TRANSFORM -1800 TO +300 NOTCH -200 TO +30
9.	APPLIED FROM 1.8 TIMES THE WATER BOTTOM 500MS AGC REMOVED
10.	EVERY OTHER CDP DROPPED TO GIVE 12.5 M CDP SPACING
11.	500MS AGC RADON DEMULTIPLE - TRANSFORM -1800 TO +300 NOTCH -200 TO +300
12.	500MS AGC REMOVED MULTIPLE VELOCITY NMO REMOVED
13.	NMO CORRECT WITH INITIAL PICKED VELOCITIES
14.	STRETCH MUTE 6HZ LOW CUT FILTER
15.	2DDMO - FK ALGORITHM
16.	PRE-STACK TIME MIGRATION USING A SINGLE MINIMUM VZ VELOCITY FUNCTION
17.	INITIAL PICKED NMO REMOVED
18.	NMO CORRECTION WITH PICKED POST PSTM VELOCITIES INNER AND OUTER TRACE MUTE
19.	2D STACK CONVENTIONAL STACK TO 1 SEC BELOW REEF TIME WEIGHTED MEDIAN STACK
20.	DIFFRACT USING A SINGLE MINIMUM VZ VELOCITY FUNCTION
21.	2D OMEGA-X MIGRATION USING 97.5 % SMOOTHED VELOCITIES
22.	TIME VARIANT FILTERING 2 SECOND BALANCE GATES OVERLAPPED BY 50 %
23.	SP 101 AT CDP 480, 6 CDPS PER SHOT SHOTPOINTS ANNOTATED AT CDP POSITION

Table 3
The predicted quantitative attributes for IVS using 2DSSM.

S. No	Thickness [m]	Porosity [%]	A I [g/c.c.*m/s]
1.	11	28	−0.089
2.	10	25	−0.08
3.	9	23	−0.067
4.	7	18	−0.07
5.	4	13	−0.053

Table 4
The predicted quantitative attributes for IVS using 2DSSDM.

S. No	Pseudo-Density [g/c.c]	Predicted Density [g/c.c]	Simulated thicknesses [m]
1.	1.8	1.8	15
2.	1.9	1.9	14.3
3.	2	2	14.4
4.	2.1	2	14.1
5.	2.2	2.1	13.2

3.4. The continuous wavelet transforms of spectral decomposition

The band-limited seismic data do not have the tuning frequency, which is used for resolving the thin-bedded reservoirs. The peak frequency in the amplitude spectrum decried the actual tuning frequency. This tuning frequency is the magnitude that can resolve the thin-bedded stratigraphic due to the highest seismic resolution at 1/4th of the wavelength and this tuning frequency [13]. Furthermore, the most constructive interference happens at this tuning frequency threshold magnitude, which also describes the petroleum system's vertical resolvable thickness. Therefore, this tuning frequency will provide accurate information, including the detection of true lithology, fluids, and the geomorphology of a complete petroleum system. Therefore, the Fourier spectrum decomposition (SD) tool is routinely applied during stratigraphic analysis. This tool provides a broad spectrum for the extraction of geometrical and physical attributes of the petroleum system. A variety of SD approaches are available. Every approach has its pros and cons. The continuous wavelet transforms (CWT) provide better imaging capability for the delineation of pure stratigraphic petroleum plays compared to the earlier SD systems [38,63]. The Gabor Morlet wavelet is the source for generating the tuning frequency volumes after the development of the designed amplitude spectrum inside the reservoir zone. The CWT method investigates a suite of abundant frequency panels [39]. The tuning frequency is picked from the peak amplitude within the designed amplitude spectrum. The CWT has proven its applicability for discriminating the vertical and lateral variability of lithologies and pore-fluid fluctuations, approximating the chronological thick-beds, and demarcating the stratigraphically trapped reserves, besides recognizing delicate frequency

distinctions that are generated by oil and gas-bearing facies [38,59,64,65].

Computationally, the CWT is the summation of the signal overall time f (t) multiplied by the scaled and shifted wavelet utility "ψ":

$$C\ (\text{Scale}, \text{translation}) = \int_{+\infty}^{-\infty} f(t)\ \psi(\text{Scale}, \text{translation}, t)dt$$

$$C\ (\sigma, \tau) = \int_{+\infty}^{-\infty} 1 \Big/ \sqrt{\sigma}\ \psi(t - \tau\ /\sigma)\ f\ (t)\ dt$$

Where the term $\sigma\ \psi(t - \tau\ /\sigma)$ is a family of scale and shifted wavelets, and σ and τ are scale and shift parameters, respectively [39].

3.4.1. CWT-based 2-D instantaneous spectral porosity geomechanical (2DSSM) and density modelling (2DSSDM)

The methodology described in Naseer [52] was developed to predict porosity for the stratigraphic traps. The same workflow is adapted for the 2DGSSM. The following key steps were applied to achieve this objective:

1. Importing the 2D seismic and well logs (GR (API, DT (microsec/ft.), Rhob (g/c.c.)) and quality control analysis.
2. Extraction of seismic amplitudes in horizontally developed pseudo-porosity wells between 7 and 29 % porosity to develop initial band-limited amplitude profile (BDP) (Fig. 4a).
3. Extraction of zero-phase seismic wavelet (Fig. 4).
4. Convolution of step 2 with step 3 to develop the resultant acoustic impedance porosity modelling (Fig. 4c).
5. Spectral decomposition-based processing within the designed amplitude spectrum (Fig. 5a).
6. Amplitude extraction within the pseudo-density cross-sections along the meandering channels (Fig. 7a).
7. Extraction of 45-Hz CWT wavelet within the zone of the reservoir at the seismic tie point of the well (Fig. 7b).
8. Convolution of steps 6 and 7 to develop the final density model (2DSSDM) (Fig. 7c).

4. Results

4.1. Seismic data interpretation

The interpretation of seismic data is a crucial component in the exploration of hydrocarbon reservoirs. Fig. 2a–c depicts the seismic database and the amplitude-based information indicating the dominant structural and stratigraphic elements of the deep-water depositional systems. The stratigraphy of this system has a moderate to high quality, characterized by a distribution of moderate amplitudes within the time frames ranging from 4.4 to 4.6 s. The reservoir development of the IVS is characterized by the trough amplitudes. It will facilitate the identification of the permeable and thickest reservoir sections of deepwater turbidities channelized deposits, which have filled the Intra-valley subsidence with facies, composed of coarse-grained sandstone. Well W-1 is identified as the development well in question, displaying a vertically logged gamma ray (API) measurement. This measurement exhibits a correlation between the filling of the internal void space and the presence of deepwater turbidities sheet-like sand (SLS), as indicated by the green-coloured line in Fig. 4b. The deposition of SLS sediments occurs during the period of sea level stability. In the vicinity immediately preceding this area, the elevation of the sea surface experiences an increase, was resulting in the deposition and accumulation of shales with high gamma-ray (GR) values, which are characteristic of the transgressive system tract (TST). The observed stratigraphic arrangement suggests the existence of a reservoir trap. Fig. 2b and c shows the prominent deep-water depositional elements of the basin. The exposure and illuminations of the meandering channel and pot bars are very close to the IVV. These channels have eroded the coarse-grained sedimentary inflexed reservoir facies from the eastern flanks. These eastern flanks are controlled by tectonic uplifting phenomena, which have developed the downthrown blocks in the western side of the basin, dominated by regional subsidence. The normal faults provided solid evidence of the subsided zone, which also connects the regional sea-level fall. This sea-level fall has created pore spaces, which have accumulated the coarse-grained sedimentary facies of point bars' primary stratigraphic traps. The eastern margins of these zones are interpreted as the erosional segments of the basin, while the western ones are suggested to be the dominant depositional segments of the petroleum systems of IMV. The onlapping stratigraphic elements further validate the onset of sea-level fall, which has created extensive pore spaces to accumulate the possible hydrocarbon-bearing reservoir sandstones.

The regional tectonics and stratigraphy can be discerned on the profile depicted in Fig. 2b. The sedimentary facies have been migrated and trapped into IVS during the folds and fault systems. The folds under consideration are linked to the strike-slip component of altered faults along the Murray Ridge. Hence, by a qualitative methodology, it is proposed that the range spanning from 35000 m to 42000 m in offset distances represents the compressional regime, whereas the range from 28000 m to 35000 m signifies the extensional regime, respectively. A multitude of sandstone lenses may have undergone migration and been caught inside the folded structure that is linked to the strike-slip component of transform boundaries. The region spanning from 28000 to 35000 m exhibits consistent sedimentation patterns along the intravertical Slope, highlighting the formation of slope areas within the basin. Folds are formed within the region commencing at an offset below 24000 m, and after their formation, the development of Internal Volcanic Structures has given rise to discrete fractures inside the IVS. The seismic amplitude profile illustrates the spatial distribution of the facies characterized by coarse-grained sandstones throughout the region. Nevertheless, it fails to accurately forecast the specific

characteristics of these deposits, including their shape, thickness, and lateral distribution.

4.2. Imaging the shelf-break architecture during sea-level fall

Fig. 2c shows the complete architecture of the deep-water depositional system, which includes the shelf-break zones at the offset location of 5560 m in the eastern margins of this basin. The tectonic uplift in the eastern flanks of the basin has initiated the uplifting followed by the downthrown blocks due to normal faulting in the westernmost and the central flanks. The concave downward with strong bright negative amplitude at the central zones of the meandering channel complex demonstrates the point bars as distinct geomorphological features at the offset locations of 12000 m and 27500 m, respectively. These curvilinear patterns confirm that the channel complex is a meander channel belt, which has pretended sufficient sedimentary influxes for filling the IMVV with the coarse-grained channelized point bar sediments into the valley. Erosion has occurred in the eastern zone up to the central zones, and caused the deposition of the sandstone-filled point bars into the IVV when the sea level was rapidly fallen, during the development of the Low stands system tract (LST). The amplitudes for the sandstone lithologies in this region are trough. This suggests that from zero to negative amplitudes zones, the sandstone will have bright negative amplitudes, reflecting the actual collations of possible gas accumulations. The sedimentary source of this IVV is the meandering channel point bar geometries, which have filled the IVV during the

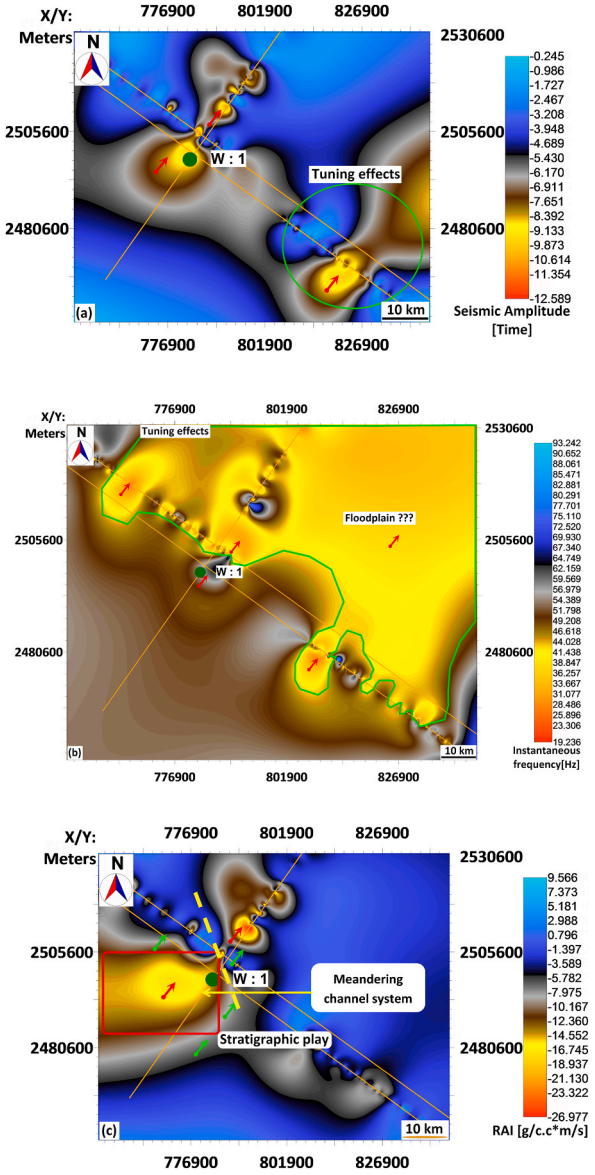

Fig. 3. Seismic attribute mapping of IVS using seismic attributes analysis. (**a**) Seismic amplitude; (**b**) Instantaneous frequency; (**c**) Relative acoustic impedance. The tuning effects are shown by green-coloured arrows and the possible reservoir zones are shown by red-coloured arrows.

extensive fall of sea level at the development of shelf-break margins. The onlapping stratigraphic features also correlate well with the regional sea-level fall. The existence of hydrocarbon-related zones can be identified by the lateral amplitude variations observed in the stratigraphy. Hence, it is imperative to employ imaging techniques to accurately assess both the spatial distribution and density of the fractured SLS deposits, since these factors serve as indicators of the reservoir quality in channelized formations. As a result, seismic attribute mapping is conducted on the IVV reservoir (Fig. 3).

4.3. Delineation of meandering channelized sandstone reservoirs within the IVS

The seismic amplitude map (SAM) displays the distribution of reservoir sandstones in the western and eastern portions of this cross-section. The Synthetic Aperture Radar (SAR) imagery illustrates two distinct forms of channel morphology within the surveyed area.

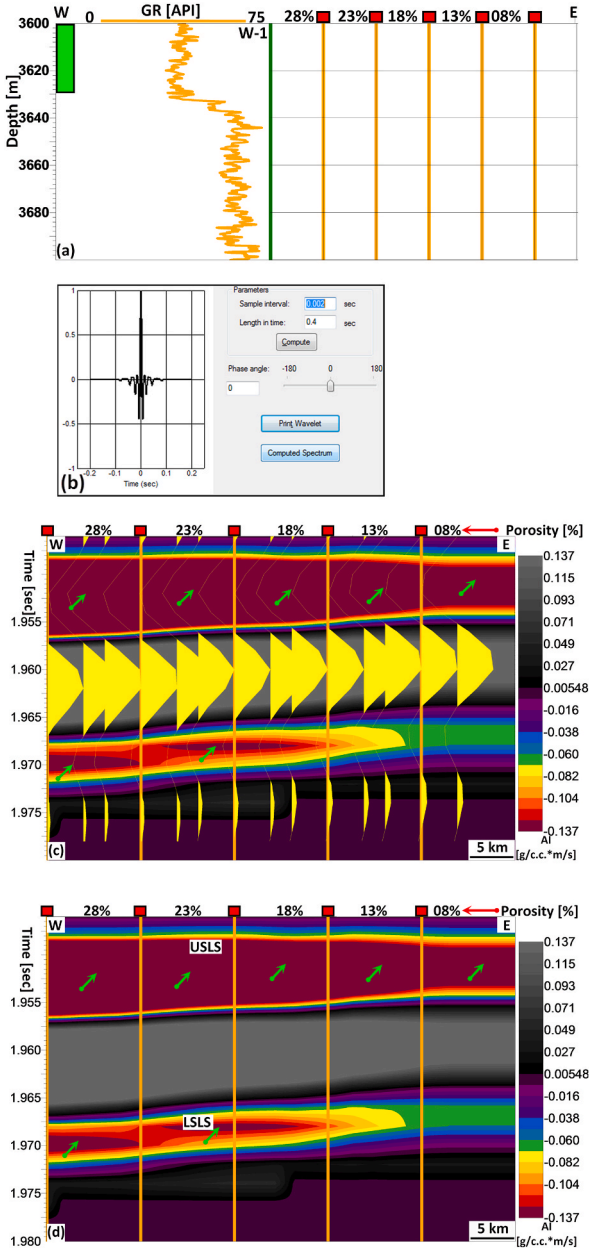

Fig. 4. Schematic development of instantaneous spectral porosity modelling. **(a)** Amplitude digitization along the pseudo-porosity wells between 7 and 29 % to develop the initial bandlimited amplitude profile (BDP); **(b)** Zero-phase seismic wavelet; **(c)** Resolute instantaneous spectral porosity model (ISPL) after convolution of step a with step b. The imposed synthetic gathers are the redeveloped synthetic seismograms to correlate the real- and predicted-impedance contrast; **(d)** The ISPL without imposed synthetic gathers.

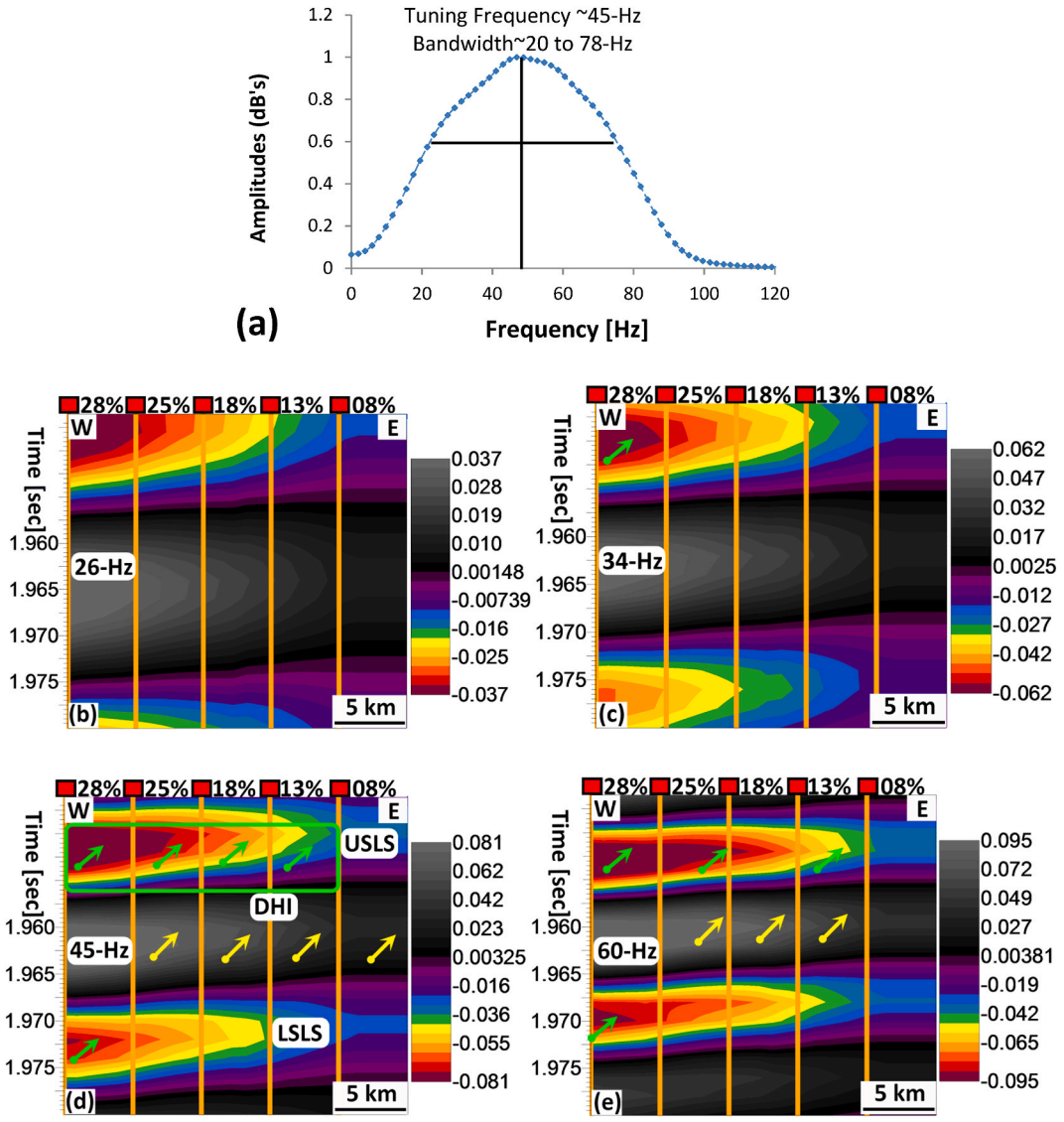

Fig. 5. **(a)** Amplitude spectrum of IVS for application of continuous wavelet transforms of spectral decomposition on ISPL in Fig. 4d into tuning frequencies (**b)** 26-Hz, (**c)** 34-Hz, (**d)** 45-Hz, (**e)** 60-Hz, respectively. The 45-Hz responds accurately in imaging the morphology and geomechanical aspects of upper sandstone lenses (Upper SLS) and lower SLS (LSLS). The reservoir sandstones (green-coloured arrows) are sealed by bottom and lateral shales (yellow-coloured arrows).

These include the presence of meandering channels in the westernmost sections, while the easternmost portions exhibit braided channels. The braided channels, which have depths ranging from −8.3 to −9.3, show a strong association with the compressional regimes observed in this petroleum system, as depicted in Fig. 3a. Hence, it may be concluded that the aforementioned channel systems lack reliability for prospective investigation, mostly because of the depletion of porosity contents resulting from sea-level rise incidents. Hence, it may be inferred that the sinuous SLS facies have deposited coarse-grained sandstone lenses within the IVS, as indicated by the red-coloured arrow in Fig. 3a. The high-amplitude anomaly is observed precisely along the W-1 zone, indicating the existence of reservoir fluids.

Fig. 3b displays the instantaneous frequency (IFY), which illustrates the lateral distribution of the reservoirs within the westernmost, easternmost, and centre zones of the IVS. The centre to northeastern and southeastern zones exhibit moderately high amplitudes (ranging from 33 to 44 Hz), which are identified as floodplain areas. The sandstone deposits of coarse grain size were subjected to erosion from the outer bends of the meandering channels. These eroded particles were then transported and deposited inside an Incised Valley System during a period of stable sea-level circumstances. It is noteworthy that the high-frequency magnitudes are recorded at the W-1, which presents a contradiction to the interpretations of seismic attributes. According to this interpretation scheme, it is expected that the regions with high amplitudes depicted in the non-seismic amplitudes map will align with the areas exhibiting low-frequency amplitudes on the IFY. Nevertheless, the flood plain exhibits amplitudes ranging from moderate to high, which aligns with

the same amplitudes observed in the Southern Annular Mode. Hence, it is imperative to validate the tuning effects, as seen in the IFY. In this regard, the Rock Amplitude Index (RAI) is employed as a means of mitigating the tuning effects caused by either inaccurate lithologies or the presence of fluids, which might obscure the well sites with high-IFY magnitudes (see Fig. 3c).

The RAI validates the two SAM-predicted interpretations of the reservoir's quality and potential for meandering and braided channel streams (Fig. 3c). There are two locations with the lowest and middle RAI amplitudes. The first location is the westernmost region of the meandering channel stream. Within this area, amplitudes are lowest (red-coloured arrow), indicating the presence of porous and coarse-grained sandstone reservoirs within the IVS. The second location is the easternmost region, which displays moderate to high negative right amplitudes (red-coloured arrow). These two zones on SAM are interpreted as clastic sandstone facies (Fig. 3a). The westernmost zones have the smallest amplitudes, validating the meandering channel system as the source of gas-bearing reservoir facies generation and accumulation within the IVS. However, braided channel streams have a greater amplitude than meandering channel streams and are therefore interpreted as having the least potential to generate and deposit gas-bearing reservoir facies within the IVS. Furthermore, these zones are influenced by compressional tectonics, and hence, the deposition of strata will also be very complex. Consequently, it is difficult to precisely anticipate the porosity, lateral distribution, thickness, and amplitude anomalies of potential gas-bearing zones. Therefore, the RAI is utilized to image the stratigraphic characteristics of this reservoir system.

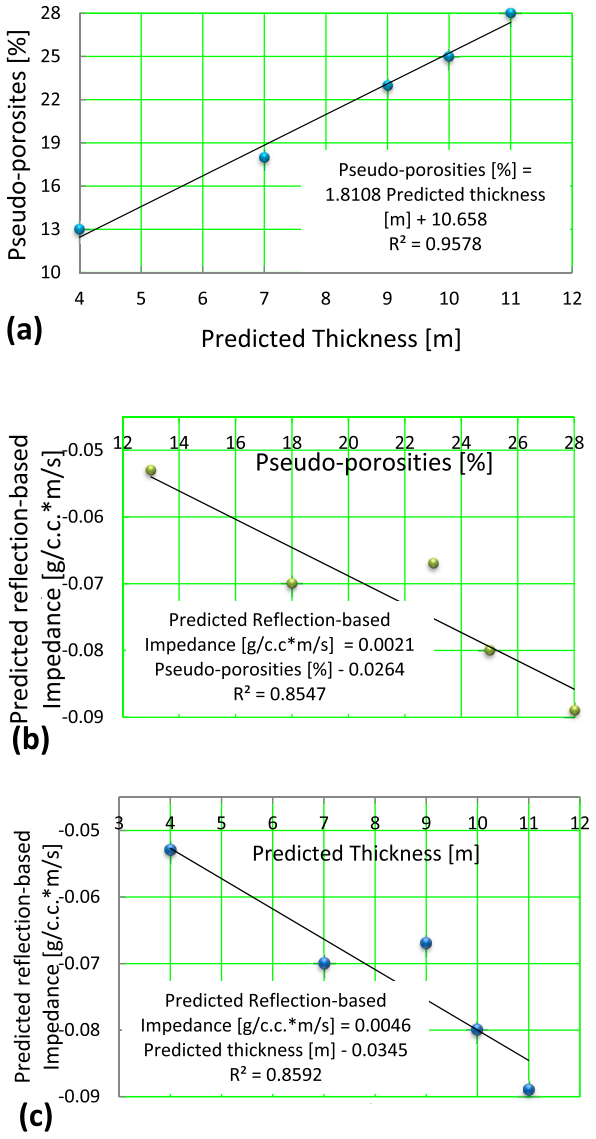

Fig. 6. Cross-plotting of predicted geomechanical parameters from ISPL in Fig. 4d. **(a)** Predicted thickness [m] versus pseudo-porosities [%], showing $R^2 > 0.95$; **(b)** Pseudo-porosities [%] versus predicted reflection-based acoustic impedance [g/c.c*m/s], showing $R^2 > 0.80$; **(c)** Predicted thickness [m] versus predicted reflection-based acoustic impedance [g/c.c*m/s], showing $R^2 > 0.80$.

The SW zone is interpreted as the depositional zone that has accumulated the most porous, coarse-grained, and thickest sandstone facies of point bars and SLS. The NE and SE zones are interpreted as erosional zones due to the meandering stream's high-velocity flow. These strike faults may have played a significant role in the lateral and vertical migration of reservoir facies and fluids. Along with the W-1 location, there is a strong indicator for the development of high-amplitude anomalies. There are numerous locations in the Miocene sequences where gas zones have been identified at various reservoir stratigraphic levels. Therefore, it is anticipated that the fluids containing gas have migrated and become confined within the IVS.

Inaccurate prediction of quantitative attributes, such as the precise orientation of fracture density, thickness, porosity, and migration of reservoir facies, is hampered by a major error in these mapping tools. These interpretations are concluded utilizing conventional seismic amplitude-based seismic attributes and W-1, which provide the lowest resolution stratigraphic attributes for this petroleum system. Consequently, these results may pertain solely to the stratigraphic gas prospect. In addition, it remains unclear how many SLS were deposited within the IVS to develop these strata as petroleum prospects. To predict these quantitative attributes, 2-D instantaneous spectral porosity modelling (2DSSM) is conducted on the premise of well and seismic data integration.

4.4. Development of 2-D instantaneous spectral porosity quantitative modelling (2DSSM) for IVS

In reservoir quality control analysis, the combination of well data and seismic characteristics is a crucial tool. The reservoir strata are significantly affected by tectonics and sea-level fluctuations [13]. As the sea level increases, the available living space decreases. Particularly in the transgressive system tract (TST), the substrates are slender or thin. To quantify these stratigraphic attributes of petroleum systems, the precise thickness, net pay zones, fracture density, depositional trends, and sideways variations in amplitudes are quantified. Point bars and channelized deposits are visible in IVS (Fig. 2a, 3a and 3c). In this kind of analysis, therefore, the integrated approach of seismic and well records is used to evaluate the reservoir quality of these primary stratigraphic traps (Figs. 4–6).

The development of reflection-based porosity modelling is outlined in section 3.2.1, providing a comprehensive description of the specific procedures involved. The pseudo-porosity wells begin by utilizing sandstone bodies that possess a tuning thickness threshold of 9 m, which is the larger thickness inside this petroleum system. Therefore, the authors generated the first band-limited amplitude profile (BDP) to delineate the reservoir zone (3600–3625 m), as shown in the green-coloured block in Fig. 4a. The extraction of the zero-phase wavelet occurs at the point of intersection between the seismic profile and the W-1 (Fig. 4b). The objective of this integration is to produce a more dependable porosity profile based on the acoustic impedance [AI], which can be used to anticipate the characteristics of thick beds, determine the precise depth of pay zones, assess fracture density, and estimate the lateral extension along the high-amplitude anomalous zones for this petroleum play. The 2DSSM is derived from the convolution of the wavelet and BDP, as seen in Fig. 4c. Fig. 4c shows the wiggled traces and Fig. 4d shows the acoustic impedance model without the wiggles. This model illustrates the presence of two significant local seismic events (SLS) occurring within the time intervals of 1.947–1.958 s and 1.964–1.974 s. The presented model demonstrates a negative correlation between acoustic impedance and porosity, indicating that an

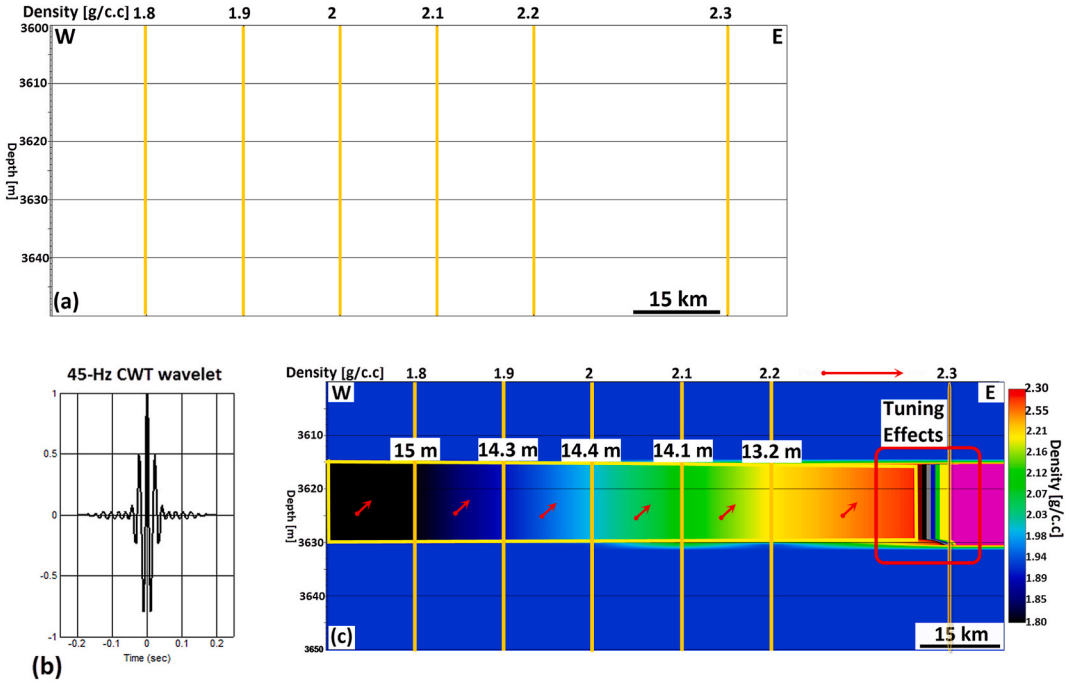

Fig. 7. Schematic approach for the development of density modelling (2DSSDM). **(a)** Amplitude extraction along the pseudo-densities of 1.8–3.2; **(b)** Extraction of 45-Hz seismic waveform; **(c)** The resultant density modelling (2DSSDM) Developed after the convolution of steps a and b.

increase in porosity is associated with a decrease in acoustic impedance. This implies that an increase in velocity will result in a decrease in the pores' space, and conversely. Consequently, the velocity parameters will be deduced from this model. The traditional or limited bandwidth (LB) 2DSSM demonstrates the homogeneous dispersion of the porous sandstone substrate. The absence of lateral variations in artificial intelligence (AI) can serve as an indication of the presence of reservoir fluids. Hence, it is imperative to disassemble the two-dimensional spectral-spatial modulation (2DSSM) into its constituent tuning frequency component before attaining the quantification of the independent variable space. The rationale for implementing this processing technique is to mitigate the inherent uncertainty that typically arises during the adjustment of shales, which can result in negative amplitudes and thus impact the visibility of the reservoir sandstone. Additionally, this will aid in verifying the processing of seismic data to ensure precise examination of oil and gas reservoirs at optimal depths and locations (Fig. 5). The displacement of reservoir SLS from their correct subsurface positions may be attributed to the impact of relative sea-level fluctuations on their vertical and lateral distribution.

4.4.1. Quantitative stratigraphic reservoir characterization

The frequency range of this spectrum spans from 20 to 78 Hz. The stratigraphic traps, such as those identified in this study are sensitive to certain frequency contents. Therefore, the bandwidth is designated for the exploration zone. Once the bandwidth is defined and the CWT is processed as performed in the reservoir simulations, the results will be suitable for extracting the information for thickness, lithology, angle of trap, and other quantitative-based attributes. Therefore, the inverted reservoir simulations are performed to predict the unknown parameters such as those developed in Figs. 4, 5 and 7. As a result, the tuning frequency has been determined to be 45 Hz. Based on the interval velocity of 1620 m/s, the vertical seismic resolution limit for this petroleum system is calculated to be 9 m. Hence, it can be deduced that the reservoir beds possess a thickness above 9 m, which is indicative of the presence of a stratigraphic structure characterized by thin beds and containing natural gas in the SLS region. Fig. 5b, c, 5d, and 5e depict the Continuous Wavelet Transform (CWT) analysis applied to the Two-Dimensional Spectral Spatial Model (2DSSM), showcasing the breakdown of spectral bandwidth ranging from 26 to 60 Hz, respectively. There exists compelling data indicating that lateral amplitudes exhibit fluctuations across varying porosities across the spectral range of 26–60 Hz. This implies that the stratigraphic SLS has been confined to the IVS, devoid of any interaction with faults.

The profile at a frequency of 26 Hz exhibits a solitary single-layered structure (SLS) during a time interval ranging from 1.933 to 1.953 s, as depicted in Fig. 5b. The model in question lacks a clearly defined bed at its base. At a frequency of 34 Hz, two significant local seismic events (SLS) may be observed in the upper and lower sections, occurring within the time intervals of 1.933–1.954 and 1.979–1.980 s (Fig. 5c). The performance of the 45-Hz model exhibits improvement, effectively addressing the structural limit states (SLS) within the time intervals of 1.933 to 1.52 s and 1.966–1.976 s (Fig. 5d). The frequency of 60 Hz is observed to exhibit two successive significant local maxima at time intervals ranging from 1.938 to 1.952 s and from 1.967 to 1.972 s, as depicted in Fig. 5e. The anticipation lies in the ability to forecast the quantitative characteristics of this system. The Upper Shallow Lacustrine System (USLS) presents itself as a viable option for investigation due to its relatively shallow depth compared to other facies. These facies have been confined inside the Internal Volcanic System (IVS). As the level of porosity escalates, there is a corresponding augmentation in the density of the fracture network inside the fractured reservoir. This phenomenon is particularly observed in point bars and channelized sandstone SLS, where the porosity is significantly enhanced. The narrowing of the trap occurs in the eastern region due to a reduction in reservoir density, indicating that it is expected to serve as the lateral sealing zone for this petroleum exploration area. Consequently, the erosional zone is anticipated to be situated at the easternmost boundary of this geological formation. The depositional zones are anticipated within the porosity zones ranging from 18 % to 28 %. The overall thickness of this underground sedimentary layer system (USLS) ranges from 9 to 13 m, indicating its suitability as a prospective option for future well drilling activities. Furthermore, to validate these outcomes effectively based on the 45-Hz profile observations, the mutual plots of the anticipated petrophysical parameters are generated to analyze the discrete level variations inside the IVS (Fig. 6).

4.4.2. Uncertainty analysis

The use of mutual plotting methodologies for the anticipated petrophysical parameters serves as a crucial instrument in the validation process and the mitigation of uncertainty in the field of oil and gas exploration. The relationship between the anticipated thickness in meters and the pseudo-porosity in percentage demonstrates a significant correlation between the projected parameters and the porosity patterns inside the IVS, as seen in Fig. 6a. The relationship between porosity and reservoir thickness is such that an increase in porosity leads to an increase in reservoir thickness. This phenomenon aligns with the fundamental principle of spectrum decomposition, which states that thin-bedded hydrocarbon-bearing traps are often detected at the tuning frequencies. The 45-Hz frequency effectively determines the precise measurements of thickness and porosity for the USLS (Fig. 6a). Table 1 displays the relevant quantitative features. The relationship between the anticipated thickness [m] and the reflection-based acoustic impedance (AI) exhibits a comparatively diminished correlation, as reflected by the R^2 value being less than 0.9, in contrast to the findings presented in Fig. 6a. Nevertheless, a coefficient of determination (R^2) over 0.85 can be characterized as significant in indicating the potential of an unconventional source of hydrocarbons, namely for oil and gas exploration. In a similar vein, there exists a strong correlation ($R^2 > 0.8$) between the projected thickness [m] and the reflection-based acoustic impedance (AI) (Fig. 6b and c). This connection implies that the accommodation space inside the internal volcanic structure (IVS) has facilitated the development of porosity, resulting in the deposition of point bars and channelized sandstone SLS with a thickness range spanning from 9 to 13 m. The thickness below this range lacks reliability for future hydrocarbon exploration due to its smaller magnitude in comparison to the tuning thickness criteria of 9 m.

4.5. CWT-based 2-D instantaneous spectral density modelling (2DSSDM)

The use of inverted density modelling has shown to be a crucial technique in the investigation of stratigraphic traps (Fig. 7a). The specific procedures are elaborated upon in Section 4.3.2. The process of extracting the initial amplitude is conducted within the density range of 1.8–2.3 g/c.c. As illustrated in Fig. 7b, the wavelet with a frequency of 45 Hz was derived from the tie point between the seismic 2D profile and well Z. The convolution procedure is utilized to generate the density inverted simulations (DM) (Fig. 7c).

The reservoir sandstone lens shows a distinct response of density inside the meandering channel body. The lateral fluctuations in the density are prominent, and there is a distinct change in the density magnitudes. These lateral fluctuations in the density magnitudes can be easily used to predict the depositional trends, thickness, lateral extent, fracture density, porosity, extensional and compressional regimes, and the types of depositional facies that are accumulated in this setting. Interestingly, this 2DSSDM shows the zone of tuning effects at 2.3 pseudo-densities well. This is the proficiency of the CWT-based wavelet, which has resolved the thin-bedded and hydrocarbon-bearing sandstone lens within the meandering channelized sandstone facies and the tuning effects. Therefore, it is suggested that the zone of pseudo-densities from 1.8 to 2.1 is the zone of deposition of coarse-grained sandstone lenses inside the meandering channels. The fracture density also increases in the western zone of the three petroleum systems. Therefore, it is suggested that the high-density zones of 2.1 and higher magnitudes have eroded the coarse-grained sandstone lenses from the eastern margins of the meandering channel and deposited them into the western zone. The western zones are also suggestive of the significant development of the accommodation space, which has accumulated the thickest and possibly porous reservoir facies inside the trap. Additionally, the eastern zones are suggested as the extensional zones, and the western zones are suggested as the compressional regimes within this petroleum system. The quantitative plots of the predicted densities and the simulated thicknesses show that the predicted densities and thicknesses are precise (Table 2; Fig. 8a and b).

These inverted density and thickness simulations may lead to the prediction of the depositional facies. There is a strong correlation between the $R^2 > 90$ for inverted densities and $R^2 > 80$ for simulated thicknesses [m]. From these two plots, the densities range from 1.8 to 2.1 g/c.c and reflect the deposition zones and dense fractured networks, which have provided the lateral migration pathways for the accumulation of 13.2–15 m thick and coarse-grained reservoir facies within the meandering channel streams. These reservoir sandstones are completely compacted from the top, bottom, and lateral shales of the transgressive system tract. Hence, these stratigraphic configurations provide for the vertical and lateral migration of the reservoir facies and the possible gas-bearing fluids inside these identified reserves. There is no fault exposure, which is observable in these facies' migrations. The lateral migration of the reservoir fluids was fault-controlled, and these migrations were not controlled by the faults. Therefore, it is suggested that pure stratigraphic traps are present inside the research zones.

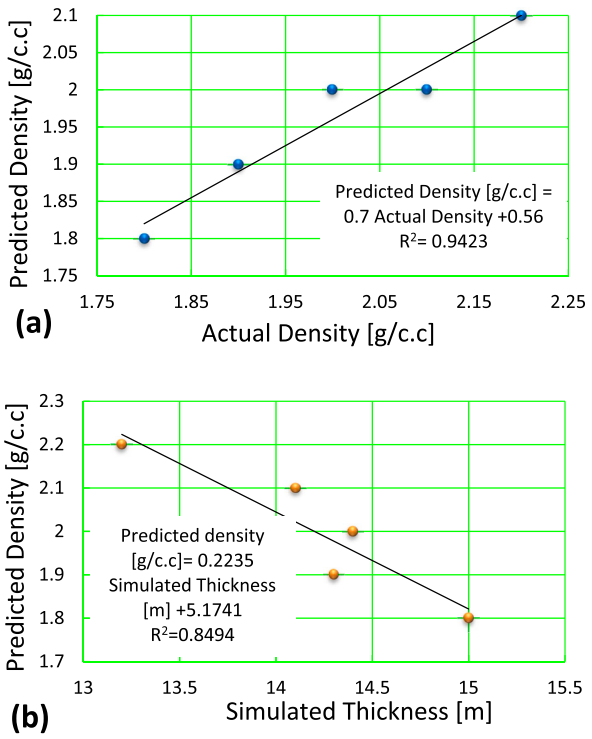

Fig. 8. Quantitative plots of predicted densities and the simulated thicknesses within the meandering channels stream. **(a)** Plot of actual and predicted densities [g/c.c]; **(b)** Plot of simulated thicknesses [m] and the predicted densities [g/c.c].

5. Discussion

The integration of seismic amplitude attributes, geophysical well logs, and inverted porosity modelling tools have revolutionized the exploration of complex depositional systems [13,52,53,66–80]. There is a variety of characteristics that have been routinely applied aimed at quantitatively and qualitatively characterizing oil and gas plays. Some of the researchers in the sub-surface characterization of diversified systems have made significant works for the development of the most sophisticated workflows such as the analysis of water level inside the drilled wells, analyzing the anomalies and ion diffusion in shale reservoirs, economic evaluation of closed-loop for the geothermal systems, spaceborne multispectral subsurface Reflectance analysis, global karst carbon sink bathymetric mapping etc. [29,74–76,81,82]. These plays can be structural, stratigraphic and/or a combination of these two regimes. The key option in this execution is to optimize the best suitable seismic attributes and inverted modelling that can provide the maximum information from the reservoirs with the least time, depth, and cost aimed at drilling wild cats. Hence, the SA, IFY, and RAI were the key seismic attributes that have been implemented to quantify the IVS. The RAI remained very successful in band-limited domains, which have provided the lateral distribution, and compared the two clastic systems of meandering channels and braided channel systems based on the AI response. The meandering channels system was provided with strong evidence for the accumulation of oil and gas-bearing reservoir fluids. The braided channel system has shown high AI, which is implicated as a poor candidate for future exploration. On the other side, the Inverted 2DSSSM has provided a more detailed and quantitative picture of the IVS for accumulating the point bars and channelized reservoir facies. However, the RAI also remained a little limited in predicting the exact thickness, and porosity, which in terms of velocity could be used for the prediction of depositional and erosional trends for the reservoir traps. At the same time, the 2DSSM has resolved the reservoirs at a thickness of 9–13 m, which was highly appreciable for future exploration. Accordingly, the conventional 2DSSSM was found to be less precise for imaging the exact depth ranges for the point bars and SLS. The 45-Hz 2DSSM has predicted the true picture of the stratigraphically trapped reserves inside the IVS (Fig. 5d), and therefore, can be considered as the key factor aimed at triumphally exploring successful oil and gas-bearing reserves.

Upon comparing the 2DSSM (Two-Dimensional Seismic Stratigraphic Model) with the 2DSSDM (Two-Dimensional Seismic Stratigraphic Density Model), it becomes apparent that the latter has successfully predicted an improved estimation of thickness. This improvement can be attributed to the utilization of convolution techniques, specifically the convolution of 45-Hz waveforms with pseudo-density wells. As a result of this convolution, the exact orientation, lateral extent, and presence of dense fractured networks within the meandering channel steam sandstone lens have been delineated. According to the 2DSSM, the anticipated thickness ranged from 9 to 12 m. The thickness of the stratigraphic traps being explored was found to range from 9 m and beyond, with a significant magnitude seen at higher values. However, the challenges arose from the fact that the reservoir formations are only drillable in the areas with the greatest thickness, where there is a significant concentration of a well-defined network and the accumulation of coarse-grained sandstone lenses inside a highly developed accommodation space. The exclusive response of the two-dimensional seismic sedimentological data (2DSSDM) accurately predicted the precise location of the coarse-grained and thin-bedded sandstone lens containing gas deposits. Additionally, it provided predictions on the seismic sedimentological characteristics, including lithology, depositional trends, and stratigraphic pinch-out zones. The significance of the impedance contrast has also contributed to the accuracy in the creation of inverted density modelling, as seen in Fig. 7c. Hence, it can be concluded that the utilization of 45-Hz inverted simulations would be the optimal approach for investigating pure stratigraphic traps throughout the Indus Basin of Pakistan.

Previously, IOB has been focused on exploration for the low-stand prograding wedge plays, which are the 25 % porous reservoirs [13,53]. The actual depths of investigations were 4000–4500 m, which is greater than those of the current study (3600–3625 m). The key differences between the previous and the current study are the investigation depth and the actual porosity values. The wedges were predicted at 25 % porous depositional settings. However, the 45-Hz has predicted a 28 % porous reservoir for shallow-marine IVS (Fig. 5c). Moreover, the tuning frequency for wedges was 48-Hz [53], which resolved 11 m thick sandstone facies. These thicknesses and porosity magnitudes are lesser than those found in the present study. Therefore, it implies that there was a more robust fall of sea level during the development of IVS compared to the wedge plays, which resolved the point bars and SLS at 13 m thickness and 28 % porosity, respectively. This workflow may also be used at the same depth of investigation to develop the IOB, which is still extensively underexplored in terms of stratigraphic traps for shallow-marine depositional environments. There are various plays in the IOB with N-block clastic depositional systems to extend this regionally stratigraphic play to more detailed geological modelling. Recently, robust attempts have been made by researchers to explore the IOB of Pakistan. A very recent development has been carried out by the explorer [48,50]. They have used the back stripping, sequence stratigraphy, and seismic amplitudes-based attributes analysis on this exploration zone. They have comprehensively identified the complete architecture elements of the deepwater depositional systems, such as the listric normal faults, compressional regimes, extensional regimes, exact orientations of faults and their generation causes, deltaic deposits, channels, and canyons. These are the key elements within the deeper water depositional sequences. The key implications of their workouts were the prediction of the seismic sequences so that they comprehensively developed the hydrocarbon trapped models. It is highly appreciable that they have used sequence stratigraphy, which is the key tool for the exploration of deepwater depositional sequences. The difference between their studies and our case study is that they have not used spectral decomposition tools. The deepwater systems are highly dependent on the gravity flow phenomenon. They certainly require tuning frequency, which resolves the thin-bedded stratigraphic traps inside the meander channel belts and basin floor fans. Additionally, they are falling behind in the prediction of the exact density and the simulation of thickness constraints (Figs. 7 and 8). It is significant to address here that both the density and thickness are the two key parameters in any deepwater exploration that can be used to predict the depositional trends in fractured networks for lateral migration of gas-bearing fluids and inside the reservoir facies (Figs. 7 and 8). These executions have been a vital tool for implicating seismic sedimentology characteristics such as the prediction lithology, frequency, phase, and impedance contrast. On this rationale, Fig. 7c shows a distinct impedance contrast between the shales and the reservoir facies, which is very

distinct in terms of discrimination of reservoir and non-reservoir zones. Additionally, the tuning frequencies of 45-Hz and its waveforms have demarcated the exact locations of the extensional compressional regimes inside the deepwater depositional system. Therefore, the 2DSSDM could have been applied to the work done by the previous researchers. Based on the conjunction of the present work and those performed by Khan and Liu [48] and Khan et al. [50], it could have explored the real locations for drilling to possible hydrocarbon-bearing and economically high-rating stratigraphic prospects inside the IOB, Pakistan.

The regional analogue for the current study is the late Miocene deep-water channel complexes in the southern Taranaki Basin, New Zealand, which were investigated using 3-D seismic datasets, spectral decomposition, amplitude curvature, and coherence attributes [83]. The attribute analysis has revealed the NW-trending straight-to-low-sinuosity channels and the less prominent NE-trending high-sinuosity feeder channels. It is highly commendable that they have used the 3D seismic data and spectral decomposition tool. It is also commendable that they have delineated a range of sinuous channel complexes using the strata slices. As the 2DSSM in our study has predicted the exact thickness, depth of the reservoir, lateral distribution of reservoirs, and fracture density (Fig. 5d), they could have used this modelling technique and post-stack processing using the tuning frequency of spectral decomposition. A little ambiguity in the work done by Silver and Bedle [83] is that they have not mentioned which type of spectral decomposition technique was used for their exportation objectives. If they have used the CWT as in our case study (Fig. 5), then it's very validating. It is so that the CWT is a better tool compared to the FFT and DFT of spectral decomposition [63], which can image the quantitative attributes of pure stratigraphic traps, such as the deepwater channel complexes in their case study [83]. Especially if the 2DSSM would be processed at their tuning frequency, it is still not clear what the tuning frequency magnitudes are, which were used by Silver and Bedle [83] to delineate the high-sinuosity channel complexes. The true frequency would surely be defined by generating the amplitude spectrum, as in our case study (Fig. 5a). Above all these observations, the porosity modelling could be inversely used for the assessment of the depositional trends and the erosional trends, which were less emphasized by these researchers [83]. Therefore, the present research may be used to enhance production by drilling on the thickest and most porous reservoir segments for oil and gas exploration in the southern Taranaki Basin, New Zealand.

5.1. Pros and cons of the proposed research work

This study utilizes the conventional amplitudes and the amplitudes-based inverted reservoir simulations for assessing the seismic stratigraphic and the seismic sedimentological response of the deep-water depositional systems (Figs. 2–4, 6). There were lots of discrepancies using the conventional seismic amplitudes as observed in Figs. 2b and 3c, where the point bars were observed, but these stratigraphic elements of deep-water depositional systems were the sub-seismic features. Even Fig. 4 could not evaluate the exact thickness and the angle of the traps, which have played a vital role in the development of these primary stratigraphic petroleum systems. However, the inverted reservoir simulations for densities and lithological porosities have made a remarkable impact on the visualizations of all these primary stratigraphic attributes, which also required a better assessment of the reservoir systems. Above all these implicated resolutions for these deepwater systems, there were some limited data sets; including the unavailability of the core and FMI logs, which was also, could have been incorporated during the research workflow. Therefore, our work is constrained to realize the more detailed reservoir architecture for the precision of lithology, faults fractures, and hydrocarbon presence. If these datasets were available in the public domain, then our research workflow could have been nourished with more accuracy and reliability. Therefore, in future research work, if these datasets were available, then these datasets would surely be applied to this study so that the Offshore Indus Basin can evolve with the highest energy recovery reserves.

5.2. 45-Hz processing and its implications on reservoir quality and hydrocarbon exploration throughout the deepwater depositional system

Spectral decomposition is a world-renowned tool for thin-bed analysis for resolving the true lithology, fluids, and faults. The fault and lithologies of the stratigraphic taps such as the channels, valley, and basin floor fans, are sub-seismic features, which are unresolvable using the conventional seismic amplitudes [54]. It depends on the objective of the research work. The stratigraphic traps such as those identified in this study are sensitive to certain frequency contents, which images and resolved as these stratigraphic traps. Therefore, the bandwidth is designated for the exploration zone. Once the bandwidth is defined and the CWT is processed as performed in the reservoir simulations, the results will be suitable for extracting the information for thickness, lithology, angle of trap, and other quantitative-based attributes [84]. The results show that the pseudo-porosities in the IOB are the most important petrophysical parameters that can help to figure out the quantitative stratigraphic properties of the thin-bed stratigraphic reservoirs. Although the RAI has been a better tool compared to the remaining full-spectrum seismic attributes for delineating the lateral distribution and morphology of the IVS, the treatment of 2DSSSM using 45-Hz frequency volumes has impacted future hydrocarbon exploration by drilling the target at the right locations.

The deepwater depositional system shows a variety of architectures, such as submarine channelized complexes, meandering channel complexes, canyons, IVS, and low-stand sandstone wedges [11,85–88]. Here, we present a very interesting case study by implementing the 2DSSSM and its processing at a 45-Hz tuning frequency. Throughout the falling of the sea and its subsequent rise, the reservoir facies and fluids migrate in a variety of pathways, including the fault, control migrated facies, and facies controlled migrated facies. In this way, it is always a challenge for exploration to determine the exact location of the reservoir, thickness, and dense fracture network for lateral and vertical migrations. The facies control migration provides robust signs aimed at the growth of stratigraphically trapped reserves within IVS. It is observed that 45-Hz-based processing of band-limited 2DSSM has demarcated the exact depth of the sandstone and shales, which implicates the presence of shale at the top of band-limited 2DSSM. The top of the sandstone at band limit 2DSSM started at 3611–3627 m. Nevertheless, the 45-Hz processed 2DSSM has shown the top of the sandstone at 3610–3624 m. The

tops and bottoms of the sandstone are different from the band-limited 2DSSM, with a difference of about 2 m, which is a huge difference. This is because the drilling cost is uncontrollable if the right targets for oil and gas exploration are not optimized. The 45-Hz 2DSSM has predicted the true thickness and depth of the reservoir of SLS in the IVS. There was no fault resolved at 45-Hz profiles, and hence, this petroleum system is developed as a pure stratigraphic play for IVS. Hence, facies migration is implicated in carried out along the facies inside the IVS. There is also a direct hydrocarbon indicator (DHI) between the depth zones of 3610 and 3624 m. Therefore, it is implied that 25–28 % of porous reservoirs have a higher potential for gas exploration compared to the porosities between 8 and 23 % zones.

6. Conclusions

The band-limited seismic attributes, such as the seismic amplitudes and IF, remained very poor in imaging the lateral extent of the SLS. The RI has imaged the excellent distribution of SLS, which has an aerial extent of 824 km^2. However, RI also remained limited in predicting the exact numbers of SLS, their vertical thicknesses, and their porosities. Therefore, the RI can be used to image the exact distribution of the reservoir sandstones. The aerial extent of the meandering channel system was 43 km^2 with the highest AI, which implies less potential for oil and gas exploration of the meandering channel system. Therefore, RAI attributes can be a fine choice for the delineation of reservoir facies, the morphology of the reservoir, and coarse-grained sedimentary facies inside the IVS.

The band-limited 2DSSM has imaged the SLS at the shallowest and deepest parts of the IVS. However, the 2DSSM has remained limited in predicting the amplitude anomaly along with the porous reservoir segments. Therefore, the 45-Hz processing has attained a very strong indicator for the presence of hydrocarbon-bearing reservoirs, which have passed through the vertical normal faults trapped inside the inner banks of the IVS. The strong $R^2 > 0.585$ has corroborated the development of pure stratigraphic traps inside the IOB in Pakistan. The deepest LSLS have attained 1–6 m with a lateral extent of 3 km within the porosity range of 18–33 %. The shallowest USLS has attained gas-bearing thick pay zones of 9–13 m with a lateral extent of 1.9 km within the porosity range of 18–33 %, which pinches out in the east and hence develops an excellent stratigraphic trap. Hence, the 45-Hz spectra and decomposition-based tuning frequency profiles can be used to predict the exact thicknesses, depths, and porosities of the SLS of the IOB, Pakistan.

The application of Continuous Wavelet Transform (CWT) in two-dimensional (2D) instantaneous spectral density modelling (2DSSDM) has successfully anticipated many geological features such as increased thickness, precise dense fractured network, depositional trends, accurate locations of extensional and compressional regimes, as well as the development and reduction accommodations. The implications discussed in this study were only derived from the utilization of the 45-Hz waveform and its convolution operation with the pseudo-densities' wells. The ramifications mentioned can be anticipated by the utilization of traditional seismic amplitude-based attribute mapping and the standard waveform-based 2DSSM. Consequently, drawing from these results, it can be inferred that the 2DSSDM exhibits potential as a superior tool for forecasting the presence of unadulterated stratigraphic traps within the IOB of Pakistan. Therefore, this process has the potential to facilitate the exploration and exploitation of untapped oil and gas reservoirs in this setting, as well as in other geological basins worldwide.

Funding

This research received has external funding.

Data availability statement

The data is available in the data resource department upon readers' request.

CRediT authorship contribution statement

Muhammad Tayyab Naseer: Writing – review & editing, Writing – original draft, Visualization, Validation, Supervision, Software, Resources, Project administration, Methodology, Investigation, Funding acquisition, Formal analysis, Data curation, Conceptualization. **Abha Singh:** Visualization, Resources. **Raja Hammad Khalid:** Visualization, Resources. **Shazia Naseem:** Visualization, Resources. **Ilyas Khan:** Visualization, Resources. **George Kontakiotis:** Visualization, Resources.

Declaration of competing interest

The authors declare that they have no known competing financial interests or personal relationships that could have appeared to influence the work reported in this paper.

Acknowledgments

Authors are thankful to the Directorate General of Petroleum Concession and Department of Earth Sciences, Quaid-I-Azam University, DGPC and LMKR for providing the research data for this study. They are also thankful to the IHS-SMT Kingdom Software support, for their excellent support and guidance during this research work.

References

[1] M.P. Gomes, H. Vital, K. Stattegger, K. Schwarzer, Bedrock control on the assu Incised Valley morphology and sedimentation in the Brazilian equatorial shelf, Int. J. Sediment Res. 31 (2016) 181–193, https://doi.org/10.1016/j.ijsrc.2015.04.002.

[2] G. De Falco, A. Carannante, C. Del Vais, L. Gasperini, V. Pascucci, I. Sanna, S. Simeone, A. Conforti, Evolution of a single incised valley related to inherited geology, sea level rise and climate changes during the Holocene (Tirso river, Sardinia, western Mediterranean Sea), Mar. Geol. 451 (2022) 106885, https://doi.org/10.1016/j.margeo.2022.106885.

[3] R. Wang, L. Colombera, N.P. Mountney, Quantitative analysis of the stratigraphic architecture of incised-valley fills: a global comparison of Quaternary systems, Earth Sci. Rev. 200 (2020) 102988, https://doi.org/10.1016/j.earscirev.2019.102988.

[4] R. Boyd, R.W. Dalrymple, B.A. Zaitlin, Estuarine and incised-valley facies models, 0, Facies Models Revisited 84 (2006), https://doi.org/10.2110/pec.06.84.0171.

[5] B.A. Zaitlin, R.W. Dalrymple, R. Boyd, The stratigraphic organization of incised-valley systems associated with relative seasea-level change, 0, Incised-Valley Systems: Origin and Sedimentary Sequences 51 (1994), https://doi.org/10.2110/pec.94.12.0045.

[6] T.J.J. Hanebuth, K. Stattegger, Depositional sequences on a late Pleistocene–Holocene tropical siliciclastic shelf (Sunda Shelf, southeast Asia), J. Asian Earth Sci. 23 (2004) 113–126, https://doi.org/10.1016/S1367-9120(03)00100-7.

[7] R.W. Dalrymple, K. Choi, Morphologic and facies trends through the fluvial–marine transition in tide-dominated depositional systems: a schematic framework for environmental and sequence-stratigraphic interpretation, Earth Sci. Rev. 81 (2007) 135–174, https://doi.org/10.1016/j.earscirev.2006.10.002.

[8] R. Boyd, W. DalrympleR, A. ZaitlinB, Estuarine and incised-valley facies models, Spec. Publ. Soc. Sediment. Geol. 84 (2006) 171–235.

[9] R.W. Dalrymple, B.A. Zaitlin, R. Boyd, Estuarine facies models; conceptual basis and stratigraphic implications, J. Sediment. Res. 62 (1992) 1130–1146.

[10] M. Mehmood, A.A. Naseem, M. Saleem, J.U. Rehman, G. Kontakiotis, H.T. Janjuhah, E.U. Khan, A. Antonarakou, I. Khan, A.U. Rehman, et al., Sedimentary facies, architectural elements, and depositional environments of the maastrichtian pab formation in the rakhi gorge, eastern sulaiman ranges, Pakistan, J. Mar. Sci. Eng. 11 (2023), https://doi.org/10.3390/jmse11040726.

[11] M.T. Naseer, Spectral decomposition' application for stratigraphic-based quantitative controls on Lower-Cretaceous deltaic systems, Pakistan: significances for hydrocarbon exploration, Mar. Petrol. Geol. 127 (2021) 104978, https://doi.org/10.1016/j.marpetgeo.2021.104978.

[12] G. Partyka, J. Gridley, J. Lopez, Interpretational applications of spectral decomposition in reservoir characterization, Lead. Edge 18 (1999) 353–360, https://doi.org/10.1190/1.1438295.

[13] M.T. Naseer, Appraisal of tectonically-influenced lowstand prograding clinoform sedimentary fairways of Early-Cretaceous Sember deltaic sequences, Pakistan using dynamical reservoir simulations: implications for natural gas exploration, Mar. Petrol. Geol. 151 (2023) 106166, https://doi.org/10.1016/j.marpetgeo.2023.106166.

[14] B. Ahmed, S. Bakht, S. Wahid, M. Hanif, Structural analysis and reservoir characterisation of cretaceous sequence in kohala bala, khyber pakhtunkhwa, Pakistan, Rudarsko-Geolosko-Naftni Zb. 37 (2022) 65–81, https://doi.org/10.17794/rgn.2022.3.6.

[15] E. Arif, J. Youliang, K. Shahzad, S. Mashwani, H. ullah, M. Zaheer, Architectural complexities and morphological variations of the sediment waves of Plio-Pleistocene channel levee backslope of the Indus Fan, Rudarsko-Geolosko-Naftni Zb. 37 (2022) 39–54, https://doi.org/10.17794/rgn.2022.2.4.

[16] D.T. Fadhil, W.A. Yonus, M.A. Theyab, Reservoir characteristics of the Miocene age formations at the allas dome, hamrin anticline, northern Iraq, Mining of Mineral Deposits 14 (2020) 17–23, https://doi.org/10.33271/mining14.04.017.

[17] W. Shang, S. Xu, X. Li, F. Liang, C. Wu, J. Wang, Z. Li, Y. Sun, Y. Li, M. Li, et al., Utilizing 2D seismic forward modeling to constrain the seismic response and plane distribution of grain shoal reservoir in the northern slope of Central Sichuan Paleo-uplift, Sichuan Basin, Mar. Petrol. Geol. 152 (2023) 106228, https://doi.org/10.1016/j.marpetgeo.2023.106228.

[18] S. Gammaldi, A. Ismail, A. Zollo, Fluid accumulation zone by seismic attributes and amplitude versus offset analysis at solfatara volcano, campi flegrei, Italy, Front. Earth Sci. 10 (2022), https://doi.org/10.3389/feart.2022.866534.

[19] O.L. Kuznetsov, I.A. Chirkin, A.A. Radwan, Combining seismic waves of different classes to enhance the efficiency of seismic exploration, in: SEG Int. Expos. 86th Ann, Meet., 2016.

[20] O.L. Kuznetsov, V.G. Gaynanov, A.A. Radwan, I.A. Chirkin, E.G. Rizanov, S.O. Koligaev, Application of scattered and emitted seismic waves for improving the efficiency of exploration and development of hydrocarbon fields, Moscow Univ. Geol. Bull. 72 (2017) 355–360, https://doi.org/10.3103/S0145875217050064.

[21] A. Ismail, H.F. Ewida, M.G. Al-Ibiary, S. Gammaldi, A. Zollo, Identification of gas zones and chimneys using seismic attributes analysis at the Scarab field, offshore, Nile Delta, Egypt, Petroleum Research 5 (2020) 59–69, https://doi.org/10.1016/j.ptlrs.2019.09.002.

[22] A. Ismail, H.F. Ewida, M.G. Al-Ibiary, S. Nazeri, N.S. Salama, S. Gammaldi, A. Zollo, The detection of deep seafloor pockmarks, gas chimneys, and associated features with seafloor seeps using seismic attributes in the West offshore Nile Delta, Egypt, Explor. Geophys. 52 (2021) 388–408, https://doi.org/10.1080/08123985.2020.1827229.

[23] A. Ismail, H.F. Ewida, S. Nazeri, M.G. Al-Ibiary, A. Zollo, Gas channels and chimneys prediction using artificial neural networks and multi-seismic attributes, offshore West Nile Delta, Egypt, J. Petrol. Sci. Eng. 208 (2022) 109349, https://doi.org/10.1016/j.petrol.2021.109349.

[24] A. Ismail, S. Gammaldi, T. Chiuso, A. Zollo, Seismic imaging of the Solfatara crater (Campi Flegrei caldera, southern Italy): new evidence of the fluids migration pathways in the shallow structures, J. Volcanol. Geoth. Res. 404 (2020) 107005, https://doi.org/10.1016/j.jvolgeores.2020.107005.

[25] A. Ismail, A.A. Radwan, M. Leila, A. Abdelmaksoud, M. Ali, Unsupervised machine learning and multi-seismic attributes for fault and fracture network interpretation in the Kerry Field, Taranaki Basin, New Zealand, Geomechanics and Geophysics for Geo-Energy and Geo-Resources 9 (2023) 122, https://doi.org/10.1007/s40948-023-00646-9.

[26] M. Elmahdy, A.A. Radwan, B.S. Nabawy, A. Abdelmaksoud, A.V. Nastavkin, Integrated geophysical, petrophysical and petrographical characterization of the carbonate and clastic reservoirs of the Waihapa Field, Taranaki Basin, New Zealand, Mar. Petrol. Geol. 151 (2023) 106173, https://doi.org/10.1016/j.marpetgeo.2023.106173.

[27] Z. Xu, X. Li, J. Li, Y. Xue, S. Jiang, L. Liu, Q. Luo, K. Wu, N. Zhang, Y. Feng, et al., Characteristics of source rocks and genetic origins of natural gas in deep formations, gudian depression, songliao basin, NE China, ACS Earth Space Chem. 6 (2022) 1750–1771, https://doi.org/10.1021/acsearthspacechem.2c00065.

[28] Z. Xi, Z. Xiaoming, G. Jiawang, L. Shuxin, Z. Tingshan, Karst topography paces the deposition of lower Permian, organic-rich, marine–continental transitional shales in the southeastern Ordos Basin, northwestern China, AAPG Bull (2023), https://doi.org/10.1306/11152322091.

[29] L. Yang, H. Wang, H. Xu, D. Guo, M. Li, Experimental study on characteristics of water imbibition and ion diffusion in shale reservoirs, Geoenergy Sci. Eng. 229 (2023) 212167, https://doi.org/10.1016/j.geoen.2023.212167.

[30] J. Yu, Y. Zhu, W. Yao, X. Liu, C. Ren, Y. Cai, X. Tang, Stress relaxation behaviour of marble under cyclic weak disturbance and confining pressures, Measurement 182 (2021) 109777, https://doi.org/10.1016/j.measurement.2021.109777.

[31] C. Ren, J. Yu, S. Liu, W. Yao, Y. Zhu, X. Liu, A plastic strain-induced damage model of porous rock suitable for different stress paths, Rock Mech. Rock Eng. 55 (4) (2022) 1887–1906, https://doi.org/10.1007/s00603-022-02775-1.

[32] W. Du, G. Wang, Intra-event spatial correlations for cumulative absolute velocity, arias intensity, and spectral accelerations based on regional site conditions, Bull. Seismol. Soc. Amer. 103 (2A) (2013) 1117–1129, https://doi.org/10.1785/0120120185.

[33] L. Yang, D. Yang, M. Zhang, S. Meng, S. Wang, Y. Su, X. Long, Application of nano-scratch technology to identify continental shale mineral composition and distribution length of bedding interfacial transition zone - A case study of Cretaceous Qingshankou formation in Gulong Depression, Songliao Basin, NE China, Geoen. Sci. Eng. 234 (2024) 212674, https://doi.org/10.1016/j.geoen.2024.212674.

[34] L. Yin, L. Wang, B.D. Keim, K. Konsoer, Z. Yin, M. Liu, W. Zheng, Spatial and wavelet analysis of precipitation and river discharge during operation of the Three Gorges Dam, China, Ecol. Indicat. 154 (2023) 110837, https://doi.org/10.1016/j.ecolind.2023.110837.

[35] C. Ren, J. Yu, X. Liu, Z. Zhang, Y. Cai, Cyclic constitutive equations of rock with coupled damage induced by compaction and cracking, Intern. J. Mining Sci. Technol. 32 (5) (2022) 1153–1165, https://doi.org/10.1016/j.ijmst.2022.06.010.

[36] C. Ren, J. Yu, C. Zhang, X. Liu, Y. Zhu, W. Yao, Micro–macro approach of anisotropic damage: A semi-analytical constitutive model of porous cracked rock, Eng. Fract. Mech. 290 (2023) 109483, https://doi.org/10.1016/j.engfracmech.2023.109483.
[37] K.J. Marfurt, R.L. Kirlin, Narrow-band spectral analysis and thin-bed tuning, Geophysics 66 (2001) 1274–1283, https://doi.org/10.1190/1.1487075.
[38] J.P. Castagna, S. Sun, R.W. Siegfried, Instantaneous spectral analysis: detection of low-frequency shadows associated with hydrocarbons, Lead. Edge 22 (2003) 120–127, https://doi.org/10.1190/1.1559038.
[39] S. Sinha, P.S. Routh, P.D. Anno, J.P. Castagna, Spectral decomposition of seismic data with continuous-wavelet transform, Geophysics 70 (2005) P19–P25, https://doi.org/10.1190/1.2127113.
[40] A. Raef, M. Totten, A. Vohs, A. Linares, 3D seismic reflection amplitude and instantaneous frequency attributes in mapping thin hydrocarbon reservoir lithofacies: morrison NE field and morrison field, clark county, KS, Pure Appl. Geophys. 174 (2017) 4379–4394, https://doi.org/10.1007/s00024-017-1664-1.
[41] A.E. Raef, M.W. Totten, A. Linares, A. Kamari, Lithofacies control on reservoir quality of the viola limestone in southwest Kansas and unsupervised machine learning approach of seismic attributes facies-classification, Pure Appl. Geophys. 176 (2019) 4297–4308, https://doi.org/10.1007/s00024-019-02205-4.
[42] A. Raef, F. Mattern, C. Philip, M. Totten, 3D seismic attributes and well-log facies analysis for prospect identification and evaluation: interpreted palaeoshoreline implications, Weirman Field, Kansas, USA, J. Petrol. Sci. Eng. 133 (2015) 40–51.
[43] J. Selvage, C. Jones, J. Edgar, Maximizing the value of 3D seismic data for shallow geohazard identification, First Break 30 (2012), https://doi.org/10.3997/1365-2397.30.8.60908.
[44] A. Chakraborty, D. Okaya, Frequency-time decomposition of seismic data using wavelet-based methods, Geophysics 60 (1995) 1906–1916, https://doi.org/10.1190/1.1443922.
[45] M.T. Naseer, Imaging of stratigraphic pinch-out traps within the lower-cretaceous shaly-sandstone system, Pakistan, using 3D quantitative seismic inverted porosity–velocity modeling, Nat. Resour. Res. 30 (2021) 4297–4327, https://doi.org/10.1007/s11053-021-09932-3.
[46] R.A. Edwards, T.A. Minshull, R.S. White, Extension across the Indian–arabian plate boundary: the Murray Ridge, Geophys. J. Int. 142 (2000) 461–477, https://doi.org/10.1046/j.1365-246x.2000.00163.x.
[47] S.M. Carmichael, S. Akhter, J.K. Bennett, M.A. Fatimi, K. Hosein, R.W. Jones, M.B. Longacre, M.J. Osborne, R.S.J. Tozer, Geology and hydrocarbon potential of the offshore Indus Basin, Pakistan, Petrol. Geosci. 15 (2009) 107–116, https://doi.org/10.1144/1354-079309-826.
[48] M. Khan, Y. Liu, Geodynamic evolution of the offshore Indus Basin Pakistan: the western Indian plate passive continental margin, Geophys. J. Int. 217 (2019) 1366–1386, https://doi.org/10.1093/gji/ggz091.
[49] M. Khan, A. Abdelmaksoud, Unfolding impacts of freaky tectonics on sedimentary sequences along passive margins: pioneer findings from western Indian continental margin (Offshore Indus Basin), Mar. Petrol. Geol. 119 (2020) 104499, https://doi.org/10.1016/j.marpetgeo.2020.104499.
[50] M. Khan, Y. Liu, A. Farid, H. Ahmed, Indications of uplift from seismic stratigraphy and backstripping of the well data in western Indus offshore Pakistan, Geol. J. 55 (2020) 553–570, https://doi.org/10.1002/gj.3425.
[51] M. Khan, Y. Liu, A. Farid, M. Owais, Characterizing seismo-stratigraphic and structural framework of late cretaceous-recent succession of offshore, Indus Pakistan 10 (2018) 174–191, https://doi.org/10.1515/geo-2018-0014.
[52] M.T. Naseer, Seismic attributes and reservoir simulation' application to image the shallow-marine reservoirs of Middle-Eocene carbonates, SW Pakistan, J. Petrol. Sci. Eng. 195 (2020) 107711, https://doi.org/10.1016/j.petrol.2020.107711.
[53] M.T. Naseer, S. Asim, P. Khalid, R.H. Khalid, Spectral decomposition application for appraisal of Miocene lowstand prograding wedge plays, Indus Offshore, Pakistan: implications for petroleum exploration, Mar. Petrol. Geol. 131 (2021) 105142, https://doi.org/10.1016/j.marpetgeo.2021.105142.
[54] M.T. Naseer, S. Naseem, R.H. Khalid, M.A. Shah, P. Khalid, Delineation of stratigraphic traps within the basin floor fans of Miocene sedimentary sequences, offshore Indus, Pakistan using inverted acoustic impedance simulations, Geol. J. 58 (2023) 722–739, https://doi.org/10.1002/gj.4620.
[55] M. Nemati, H. Pezeshk, Spatial distribution of fractures in the asmari formation of Iran in subsurface environment: effect of lithology and petrophysical properties, Nat. Resour. Res. 14 (2005) 305–316, https://doi.org/10.1007/s11053-006-9000-y.
[56] F.D. Gray, P.F. Anderson, J.A. Gunderson, Prediction of shale plugs between wells in heavy oil sands using seismic attributes, Nat. Resour. Res. 15 (2006) 103–109, https://doi.org/10.1007/s11053-006-9009-2.
[57] K.D. Oyeyemi, M.T. Olowokere, A.P. Aizebeokhai, Prospect analysis and hydrocarbon reservoir volume estimation in an exploration field, shallow offshore depobelt, western Niger delta, Nigeria, Nat. Resour. Res. 28 (2019) 173–185, https://doi.org/10.1007/s11053-018-9377-4.
[58] M.T. Taner, Seismic Attributes, vol. 26, Canadian Society of Exploration Geophysicists, Recorder, 2001, pp. 48–56.
[59] M.T. Naseer, S. Asim, Application of instantaneous spectral analysis and acoustic impedance wedge modeling for imaging the thin beds and fluids of fluvial sand systems of Indus Basin, Pakistan, J. Earth Syst. Sci. 127 (2018) 97, https://doi.org/10.1007/s12040-018-0997-1.
[60] M.T. Taner, F. Koehler, R.E. Sheriff, Complex seismic trace analysis, Geophysics 44 (1979) 1041–1063, https://doi.org/10.1190/1.1440994.
[61] A.R. Brown, Understanding seismic attributes, Geophysics 66 (2001) 47–48, https://doi.org/10.1190/1.1444919.
[62] R.S.C. Cobbold, Foundations of Biomedical Ultrasound, Oxford University Press, 2007.
[63] J.P. Castagna, S. Sun, Comparison of spectral decomposition methods, First Break 24 (2006), https://doi.org/10.3997/1365-2397.24.1093.26885.
[64] M.N. Tayyab, S. Asim, Application of spectral decomposition for the detection of fluvial sand reservoirs, Indus Basin, SW Pakistan, Geosci. J. 21 (2017) 595–605, https://doi.org/10.1007/s12303-017-0003-y.
[65] M.T. Naseer, S. Asim, Characterization of shallow-marine reservoirs of Lower Eocene carbonates, Pakistan: continuous wavelet transforms-based spectral decomposition, J. Nat. Gas Sci. Eng. 56 (2018) 629–649, https://doi.org/10.1016/j.jngse.2018.06.010.
[66] S. Chopra, K.J. Marfurt, Seismic attributes — a historical perspective, Geophysics 70 (2005) 3–28.
[67] G.O. Emujakporue, E.E. Enyenihi, Identification of seismic attributes for hydrocarbon prospecting of Akos field, Niger Delta, Nigeria, SN Appl. Sci. 2 (2020) 910, https://doi.org/10.1007/s42452-020-2570-1.
[68] Y. Liang, C. Li, Y. Song, Application of seismic instantaneous attributes in gas reservoir prediction, IOP Conf. Ser. Earth Environ. Sci. 237 (2019) 032070, https://doi.org/10.1088/1755-1315/237/3/032070.
[69] S. Jia, Z. Dai, Z. Zhou, H. Ling, Z. Yang, L. Qi, Z. Wang, X. Zhang, H.V. Thanh, M.R. Soltanian, Upscaling dispersivity for conservative solute transport in naturally fractured media, Water Res. 235 (2023) 119844, https://doi.org/10.1016/j.watres.2023.119844.
[70] L. Yin, L. Wang, J. Li, S. Lu, J. Tian, Z. Yin, S. Liu, W. Zheng, YOLOV4_CSPBi: enhanced land target detection model, Land 12 (2023), https://doi.org/10.3390/land12091813.
[71] L. Yin, L. Wang, T. Li, S. Lu, J. Tian, Z. Yin, X. Li, W. Zheng, U-Net-LSTM: time series-enhanced lake boundary prediction model, Land 12 (2023), https://doi.org/10.3390/land12101859.
[72] H. Yu, H. Wang, Z. Lian, An assessment of seal ability of tubing threaded connections: a hybrid empirical-numerical method, J. Energy Resour. Technol. 145 (2022), https://doi.org/10.1115/1.4056332.
[73] Y. Tie, X. Rui, S.-H. Sun, Z.-K. Hou, J.-Y. Feng, A real-time intelligent lithology identification method based on a dynamic felling strategy weighted random forest algorithm, Petrol. Sci. (2023).
[74] G. Zhou, S. Su, J. Xu, Z. Tian, Q. Cao, Bathymetry retrieval from spaceborne multispectral subsurface reflectance, IEEE J. Sel. Top. Appl. Earth Obs. Rem. Sens. 16 (2023) 2547–2558, https://doi.org/10.1109/JSTARS.2023.3249789.
[75] B. Jia, G. Zhou, Estimation of global karst carbon sink from 1950s to 2050s using response surface methodology, Geo-Spatial Inf. Sci. (2023) 1–18, https://doi.org/10.1080/10095020.2023.2165974.
[76] J. Xu, G. Zhou, S. Su, Q. Cao, Z. Tian, The development of A rigorous model for bathymetric mapping from multispectral satellite-images, Rem. Sens. 14 (10) (2022), https://doi.org/10.3390/rs14102495.
[77] J. Li, Y. Zhang, L. Lin, Y. Zhou, Study on the shear mechanics of gas hydrate-bearing sand-well interface with different roughness and dissociation, Bull. Eng. Geol. Environ. 82 (2023) 404, https://doi.org/10.1007/s10064-023-03432-9.
[78] Y. Wang, J. Peng, L. Wang, C. Xu, B. Dai, Micro-macro evolution of mechanical behaviors of thermally damaged rock: a state-of-the-art review, J. Rock Mech. Geotech. Eng. (2023), https://doi.org/10.1016/j.jrmge.2023.11.012.

[79] F.-q. Su, X.-l. He, M.-j. Dai, J.-n. Yang, A. Hamanaka, Y.-h. Yu, W. Li, J.-y. Li, Estimation of the cavity volume in the gasification zone for underground coal gasification under different oxygen flow conditions, Energy 285 (2023) 129309, https://doi.org/10.1016/j.energy.2023.129309.
[80] J. Lyu, L. Huang, L. Chen, Y. Zhu, S. Zhuang, Review on the terahertz metasensor: from featureless refractive index sensing to molecular identification, Photon. Res. 12 (2024) 194–217, https://doi.org/10.1364/PRJ.508136.
[81] H. Yin, Q. Wu, S. Yin, S. Dong, Z. Dai, M.R. Soltanian, Predicting mine water inrush accidents based on water level anomalies of borehole groups using long short-term memory and isolation forest, J. Hydrol. 616 (2023) 128813, https://doi.org/10.1016/j.jhydrol.2022.128813.
[82] D. Xiao, M. Liu, L. Li, X. Cai, S. Qin, R. Gao, G. Li, Model for economic evaluation of closed-loop geothermal systems based on net present value, Appl. Therm. Eng. 231 (2023) 121008, https://doi.org/10.1016/j.applthermaleng.2023.121008.
[83] C. Silver, H. Bedle, Evolution of a late Miocene deep-water depositional system in the southern Taranaki Basin, New Zealand, Geosciences 11 (2021), https://doi.org/10.3390/geosciences11080329.
[84] M.T. Naseer, S. Naseem, A. Singh, P. Khalid, A.E. Redwan, W. Li, F. Muhammad Faisal Rafiq, I. Khan, A. Abd El Aal, H. Al-Awah, et al., Seismic attributes and spectral decomposition-based inverted porosity-constrained simulations for appraisal of shallow-marine lower-Cretaceous sequences of Miano gas field, Southern Pakistan, Heliyon 10 (2024) e25907, https://doi.org/10.1016/j.heliyon.2024.e25907.
[85] W.L. Fisher, W.E. Galloway, R.J. Steel, C. Olariu, C. Kerans, D. Mohrig, Deep-water depositional systems supplied by shelf-incising submarine canyons: recognition and significance in the geologic record, Earth Sci. Rev. 214 (2021) 103531, https://doi.org/10.1016/j.earscirev.2021.103531.
[86] L.A.S. Hansen, D.M. Hodgson, A. Pontén, D. Bell, S. Flint, Quantification of basin-floor fan pinchouts: examples from the karoo basin, South Africa, Front. Earth Sci. 7 (2019), https://doi.org/10.3389/feart.2019.00012.
[87] L.A.S. Hansen, R.S. Healy, L. Gomis-Cartesio, D.R. Lee, D.M. Hodgson, A. Pontén, R.J. Wild, The origin and 3D architecture of a km-scale deep-water scour-fill: example from the skoorsteenberg Fm, karoo basin, South Africa, Front. Earth Sci. 9 (2021), https://doi.org/10.3389/feart.2021.737932.
[88] S. Rodrigues, F.J. Hernández-Molina, R.D. Larter, M. Rebesco, C.D. Hillenbrand, R.G. Lucchi, F.J. Rodríguez-Tovar, Sedimentary model for mixed depositional systems along the Pacific margin of the Antarctic Peninsula: decoding the interplay of deep-water processes, Mar. Geol. 445 (2022) 106754, https://doi.org/10.1016/j.margeo.2022.106754.